Research Paper

GEOSPHERE

GEOSPHERE, v. 17

https://doi.org/10.1130/GES02370.1

7 figures (2 are interactive); 1 table;
1 set of supplemental files

CORRESPONDENCE:
hampel@geowi.uni-hannover.de

CITATION: Hampel, A., Hetzel, R., and Erdmann, M.-S., 2021, Postglacial slip distribution along the Teton normal fault (Wyoming, USA), derived from tectonically offset geomorphological features: Geosphere, v. 17, https://doi.org/10.1130/GES02370.1.

Science Editor: David E. Fastovsky
Associate Editor: Andrew V. Zuza

Received 19 November 2020
Revision received 7 March 2021
Accepted 10 May 2021

GOLD OPEN ACCESS

THE GEOLOGICAL SOCIETY OF AMERICA®

This paper is published under the terms of the CC-BY-NC license.

© 2021 The Authors

Postglacial slip distribution along the Teton normal fault (Wyoming, USA), derived from tectonically offset geomorphological features

Andrea Hampel[1,*], Ralf Hetzel[2], and Maria-Sophie Erdmann[2]

[1]Institut für Geologie, Leibniz Universität Hannover, Callinstr. 30, 30167 Hannover, Germany
[2]Institut für Geologie und Paläontologie, Westfälische Wilhelms-Universität Münster, Corrensstr. 24, 48149 Münster, Germany

ABSTRACT

Along the eastern front of the Teton Range, northeastern Basin and Range province (Wyoming, USA), well-preserved fault scarps that formed across moraines, river terraces, and other geomorphological features indicate that multiple earthquakes ruptured the range-bounding Teton normal fault after the Last Glacial Maximum (LGM). Here we use high-resolution digital elevation models derived from lidar data to determine the vertical slip distribution along strike of the Teton fault from 54 topographic profiles across tectonically offset geomorphological features along the entire Teton Range front. We find that offset LGM moraines and glacially striated surfaces show higher vertical displacements than younger fluvial terraces, which formed at valley exits upstream of LGM terminal moraines. Our results reveal that the tectonic offsets preserved in the fault scarps are post-LGM in age and that the postglacial slip distribution along strike of the Teton fault is asymmetric with respect to the Teton Range center, with the maximum vertical displacements (27–23 m) being located north of Jenny Lake and along the southwestern shore of Jackson Lake. As indicated by earlier three-dimensional numerical models, this asymmetric slip distribution results from postglacial unloading of the Teton fault, which experienced loading by the Yellowstone ice cap and valley glaciers in the Teton Range during the last glaciation.

1. INTRODUCTION

Determining the slip rates of active faults or the slip associated with paleoearthquakes is an essential step in paleoseismology and seismic hazard analysis (Schwartz and Coppersmith, 1984; McCalpin, 2009). The activity of normal and thrust faults commonly leads to the formation of fault scarps due to the displacement of landforms such as fluvial terraces, moraines, or alluvial fan surfaces (e.g., Bucknam and Anderson, 1979; Hanks and Andrews, 1989). Fault scarps therefore preserve information about cumulative coseismic slip from former earthquakes (Gilbert, 1884; Schwartz and Coppersmith, 1984; Machette et al., 1991; Avouac and Peltzer, 1993; McCalpin and Nishenko, 1996; Hetzel et al., 2004a). If scarps are laterally continuous along a fault, they may also provide the opportunity to constrain the along-strike fault displacement profile, which allows extracting information on the displacement-length ratio and ultimately on the slip evolution of the fault (e.g., Cowie and Scholz, 1992; Philip et al., 1992; Dawers et al., 1993; Schlische et al., 1996; Roberts and Michetti, 2004; Manighetti et al., 2005). Ideally, fault displacement profiles have a parabolic shape, with the displacement reaching its maximum near the fault center and decreasing toward the fault tips (Cowie and Scholz, 1992). This parabolic shape may also be reflected in the topography created by the dip-slip movement of the fault at depth, in which case topographic profiles along the crest of fault-bounded mountain range can be interpreted as an expression of the cumulative fault displacement profile (e.g., Densmore et al., 2004; Hetzel et al., 2004b; Amos et al., 2010). Deviations from a parabolic displacement profile may indicate, for example, a slip deficit at a fault segment boundary or lateral variations in rock properties (Dawers et al., 1993; Anders and Schlische, 1994; Schlische et al., 1996; Manighetti et al., 2004). In addition, an external forcing like glacial loading or postglacial unloading can cause along-strike variations in fault slip rates, which may ultimately lead to the development of an asymmetric displacement profile, especially if the load is located along strike of a dip-slip fault (e.g., Hampel et al., 2009).

A prominent example of a fault that experienced such asymmetric glacial loading is the Teton normal fault in the northeastern Basin and Range province (Wyoming, USA) (Fig. 1). During the LGM (Pinedale glaciation), the valleys of the Teton Range were filled by glaciers with a thickness of several hundred meters (Love et al., 2003; Licciardi and Pierce, 2008, 2018). In addition, the northern part of the Teton fault was covered by the southern lobes of the Yellowstone ice cap, which reached a thickness of ~1 km farther north on the Yellowstone Plateau (Love et al., 2003; Licciardi and Pierce, 2008, 2018). Numerical modeling predicted that the melting of the ice cap and valley glaciers at the end of the Pinedale glaciation (ca. 15–14 ka) caused a phase of accelerated slip on the Teton fault, with two-thirds of the total postglacial slip occurring before 8 ka (Hampel et al., 2007). The model results also showed considerable along-strike variations in the fault slip rate due to the laterally variable ice cover, with rates being almost twice as high in the northern and central fault sections as in the southern section. Despite the presence of well-preserved postglacial fault scarps along almost the entire length of the Teton fault, however, it has never been investigated whether the laterally variable slip acceleration has resulted in an asymmetric along-strike slip distribution. Rather,

Andrea Hampel https://orcid.org/0000-0001-8508-8918

Downloaded from http://pubs.geoscienceworld.org/gsa/geosphere/article-pdf/doi/10.1130/GES02370.1/5364509/ges02370.pdf
by Technische Informationsbibliothek (TIB) user

previous studies focused on analyzing the scarps in the central and southern fault sections and used scarp height and/or vertical separation as proxies for vertical slip (Byrd et al., 1994; Byrd, 1995; O'Connell et al., 2003; Thackray and Staley, 2017; see section 2.1 for a summary). However, as explained in the next paragraph, neither scarp height nor vertical separation are reliable approximations of vertical slip, especially if the scarps formed across landforms with steep and highly variable slope angles as found along the Teton Range front.

A common way to estimate the vertical slip recorded by a fault scarp is to analyze topographic profiles across tectonically offset geomorphological markers (e.g., Schwartz and Coppersmith, 1984; Avouac and Peltzer, 1993; McCalpin, 2009). From such profiles, the scarp height H and the vertical separation Δz of the tectonically offset geomorphic marker can be obtained (Fig. 2, insets). Commonly, the vertical separation is used as an approximation for the vertical slip on the underlying fault. However, even for pure dip-slip faults and planar markers with the same strike as the fault underneath, the vertical separation Δz is not the same as the vertical slip S_z (Fig. 2) (Caskey, 1995; Thompson et al., 2002; Mackenzie and Elliott, 2017). For a downhill-facing scarp of a normal fault, for example, the vertical slip S_z is larger than the vertical separation Δz and can be quantified as $S_z = \Delta z / (1 - \cot\delta \tan\theta_f)$ if the fault dip δ and the far-field slope θ_f are known (Fig. 2A) (e.g., Caskey, 1995; Mackenzie and Elliott, 2017). Importantly, the ratio of $S_z/\Delta z$ increases with increasing far-field slope θ_f (Fig. 2A). For an uphill-facing normal fault scarp, the vertical slip S_z is smaller than the vertical separation Δz and can be calculated from $S_z = \Delta z / (1 + \cot\delta \tan\theta_f)$ (Fig. 2B). In this case, the ratio of $S_z/\Delta z$ is ≤1 and decreases within increasing slope (Fig. 2B). The relation between scarp height H and vertical slip S_z is even more complex because H increases with time as the scarp degrades and the maximum slope angle of the scarp (θ_s) decreases (Fig. 2A, inset) (e.g., McCalpin, 2009). The larger the far-field slope, the larger the discrepancy between scarp height and vertical separation. For downhill-facing scarps, the scarp height can therefore be regarded as only an upper bound for the vertical separation. For uphill-facing scarps, the scarp height underestimates the vertical separation. In summary, the approach of using the vertical separation (or simply the scarp height) as an approximation for the vertical fault slip is justified only if the surface slope of the offset geomorphological marker does not exceed a few degrees. If this precondition is not fulfilled, the vertical slip needs to be determined from the vertical separation and the far-field slope using the equations described above (Caskey, 1995; Thompson et al., 2002; Mackenzie and Elliott, 2017).

In this study, we analyze altogether 54 topographic profiles across the well-preserved scarps of the Teton fault to constrain, for the first time, the postglacial vertical slip distribution along its entire length. For our analysis, we use high-resolution digital elevation models (DEMs) derived from lidar data (Zellman et al., 2019), which reveal the fault scarps and the characteristics of the different offset geomorphological features including moraines, glacial surfaces, and fluvial terraces in great detail. We derive the vertical slip S_z from the vertical separation using the above-mentioned relationships, thereby taking into account the highly variable far-field slopes (see Section 3). With this approach, the effect of lateral variations in the far-field slope on the slip estimates is eliminated, which allows us to compare the actual vertical slip recorded by the different landforms. Based on our results, we conclude that all tectonic offsets recorded by the Teton fault scarps represent the cumulative slip after the Last Glacial Maximum (LGM) and that the Teton fault exhibits an asymmetric postglacial displacement profile, which can be related to the postglacial unloading of the Teton-Yellowstone region. Our comprehensive

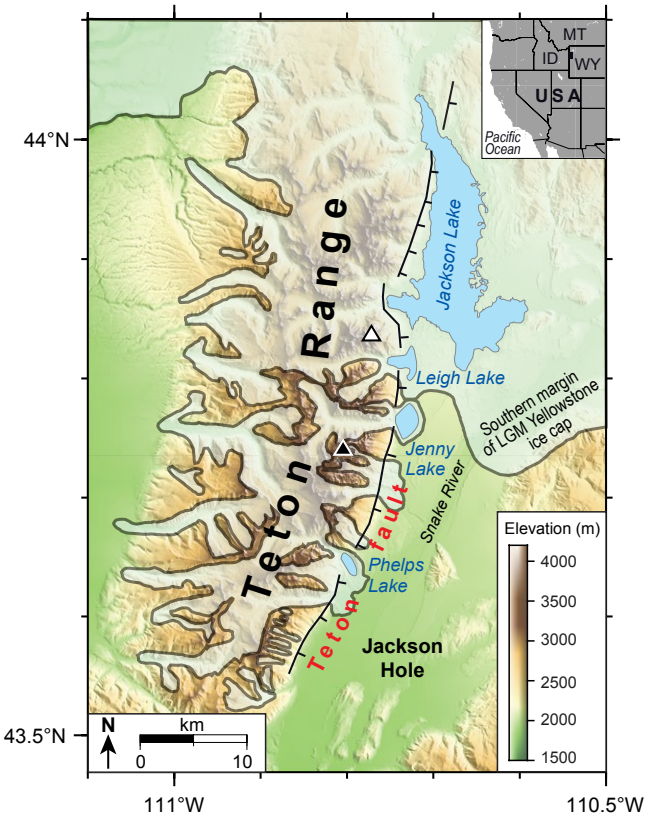

Figure 1. Location map of the Teton Range (Wyoming, USA) with the simplified surface trace of the Teton fault (black solid line with bars on downthrown side). Black and white triangles mark the peaks of Grand Teton (4197 m) and Mount Moran (3842 m), respectively. Transparent white area with gray outline marks the southern extent of the Last Glacial Maximum (LGM) Yellowstone ice cap, which reached a thickness of ~1 km farther north on the Yellowstone Plateau, and of the LGM Teton Range valley glaciers, which reached ice thicknesses of several hundred meters (Love, 2003; Licciardi and Pierce, 2018). Note that Jenny Lake is located at the southern margin of the former Yellowstone ice cap (Licciardi and Pierce, 2018). ID—Idaho; MT—Montana; WY—Wyoming.

Downloaded from http://pubs.geoscienceworld.org/gsa/geosphere/article-pdf/doi/10.1130/GES02370.1/5364509/ges02370.pdf
by Technische Informationsbibliothek (TIB) user

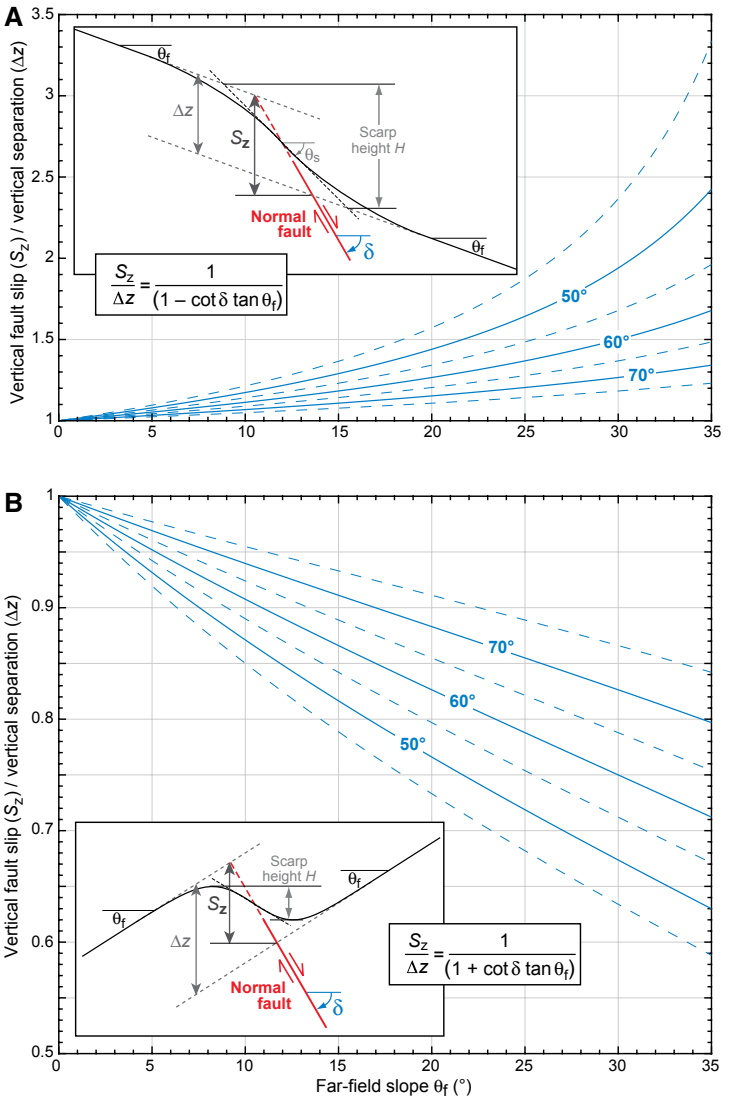

Figure 2. Relationship between (1) the ratio of the vertical fault slip S_z to the vertical separation Δz and (2) the far-field slope θ_f for different fault dips δ (blue curves) for a downhill-facing (A) and uphill-facing (B) normal fault scarp. Other parameters are: H—scarp height; θ_s—maximum slope of the scarp.

data set provides a base for calculating vertical fault slip rates as more age constraints for the different landforms become available along the Teton Range front (e.g., Licciardi and Pierce, 2018; Pierce et al., 2018) and for future numerical models that will incorporate these age constraints and recently published data on the Teton fault earthquake history (Larsen et al., 2019; DuRoss et al., 2020, 2021; Zellman et al., 2020; see Section 2.2).

2. GEOLOGICAL SETTING AND PREVIOUS WORK

The ~72-km-long Teton fault is a seismically active normal fault located in the northeastern Basin and Range province (Fig. 3). It runs along the base of the eastern flank of the Teton Range, which is renowned for its high topography and relief. The highest peak, the Grand Teton (4197 m), is located in the center of the range and stands ~2400 m above the adjacent basin of Jackson Hole in the east. Both elevation and relief of the Teton Range decrease to the north and south and are roughly symmetric with respect to the range center that is located near Jenny Lake.

The onset of activity along the Teton fault, which accommodates east-west to southwest-northeast extension (Machette et al., 2001; Puskas et al., 2007; White et al., 2009), is still under debate. Faulting may have started before 10 Ma with fault slip reaching as much as 9 km, or after 2 Ma with a total fault slip of <3 km (Love, 1977; Roberts and Burbank, 1993; Smith et al., 1993; Byrd et al., 1994; Morgan and McIntosh, 2005; Pierce and Morgan, 2009). Recent thermochronological studies in the Teton Range suggest that the onset of rapid cooling (which may be considered as a proxy for fault movement) began at ca. 15–13 Ma in the Mount Moran area in response to Basin and Range extension (Brown et al., 2017; Hoar, 2019). As a consequence of the diverse estimates for timing and amount of slip on the Teton fault, estimates for the long-term vertical slip rate of the Teton fault vary from 0.5 to 1.2 mm/yr.

During the LGM (Pinedale glaciation), the Teton Range was heavily glaciated and its deep U-shaped valleys were occupied by glaciers, while the southern lobes of the Yellowstone ice cap extended to the central part of the Teton fault near Jenny Lake (Fig. 3). Published and preliminary ^{10}Be exposure ages for moraines and glacially scoured bedrock show that the glaciers retreated rapidly from the Teton mountain front at ca. 16–14 ka (Licciardi and Pierce, 2018; Pierce et al., 2018). As constrained by radiocarbon dating, sedimentation in Jenny Lake commenced at ca. 14 ka (Larsen et al., 2019).

2.1 Fault Scarps along the Teton Normal Fault and Previous Scarp Analyses

The seismic activity of the Teton fault since the end of the Pinedale glaciation (i.e., after ca. 15–14 ka) is recorded by fault scarps, which are present almost along the entire length of the fault and formed across lateral moraines, bedrock surfaces with macroscale glacial striations, alluvial fans, and fluvial

Downloaded from http://pubs.geoscienceworld.org/gsa/geosphere/article-pdf/doi/10.1130/GES02370.1/5364509/ges02370.pdf
by Technische Informationsbibliothek (TIB) user

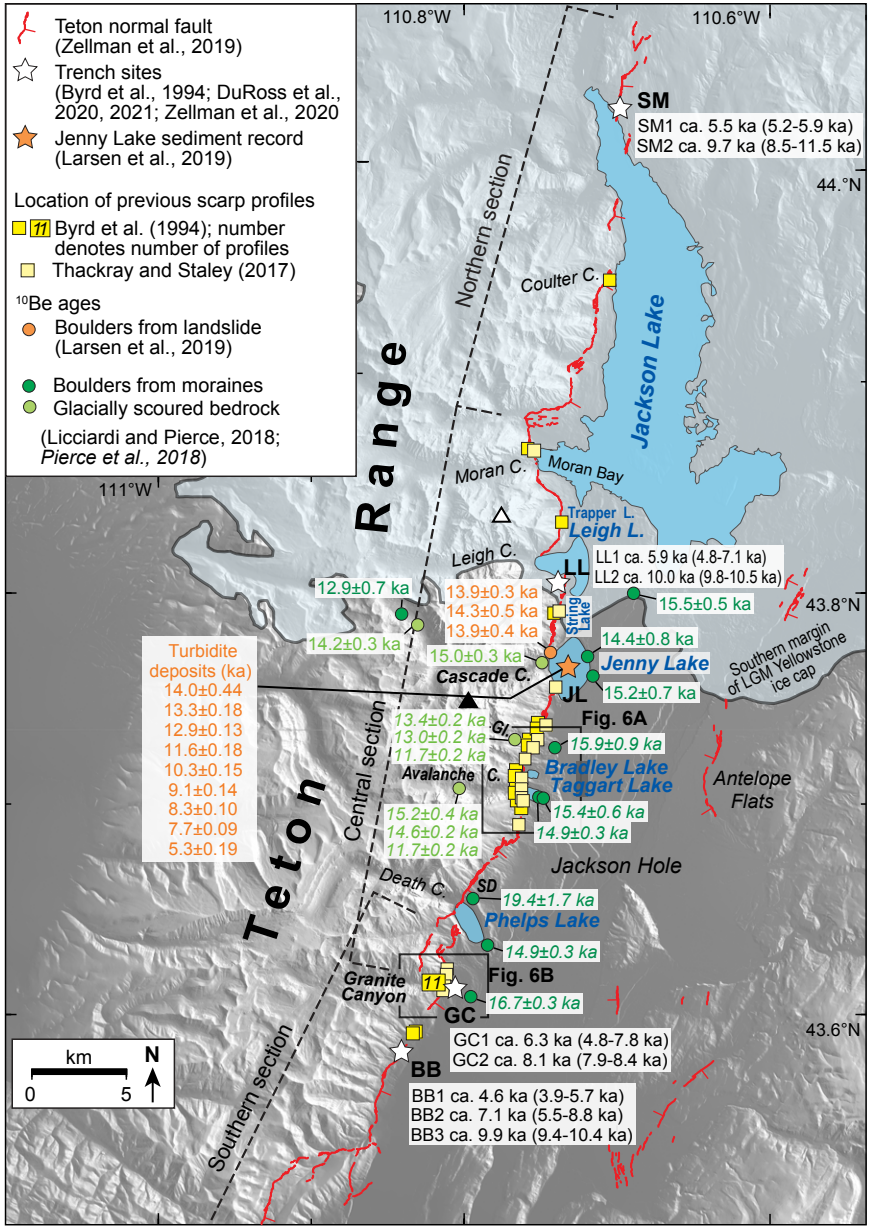

Figure 3. Map showing the detailed surface traces of the Teton fault and Jackson Hole intrabasin faults (red solid line with bars on downthrown side; from Zellman et al., 2019). Dashed black lines outline the northern, central, and southern sections of the Teton fault, respectively (after DuRoss et al., 2021). Transparent white area with gray outline marks the southern extent of the Last Glacial Maximum (LGM) Yellowstone ice cap (Licciardi and Pierce, 2018). White stars indicate the location of paleoseismological trench sites (GC—Granite Canyon [Byrd et al., 1994]; BB—Buffalo Bowl [DuRoss et al., 2020]; LL—Leigh Lake [Zellman et al., 2020]; SM—Steamboat Mountain [DuRoss et al., 2021]). Orange star and circle mark the location of the Jenny Lake (JL) sediment record and dated landslide boulders, respectively (Larsen et al., 2019). Dark and light green circles indicate locations where ^{10}Be exposures ages have been determined for moraines and glacially scoured bedrock, respectively (Licciardi and Pierce, 2018; preliminary ages from Pierce et al. [2018] are shown in italics). Yellow squares mark the locations where Byrd et al. (1994) and Thackray and Staley (2017) determined scarp height and vertical separation values from scarp profiles. Dark gray rectangles indicate areas shown in Figures 6B and 6C. C.—Canyon; L.—Lake; Gl—Glacier Gulch; SD—Stewart Draw. Black and white triangles mark the peaks of Grand Teton (4197 m) and Mount Moran (3842 m), respectively.

Downloaded from http://pubs.geoscienceworld.org/gsa/geosphere/article-pdf/doi/10.1130/GES02370.1/5364509/ges02370.pdf
by Technische Informationsbibliothek (TIB) user

terraces (Love et al., 1992; Byrd et al., 1994; Licciardi and Pierce, 2008, 2018; Pierce et al., 2018; Zellman et al., 2019). The height of these scarps reaches >35 m near the range center at String Lake and generally decreases to the north and south, although there are also pronounced lateral variations (Byrd et al., 1994; Thackray and Staley, 2017).

In the past, several studies used topographic profiles across the scarps of the Teton fault to measure scarp height and vertical separation (Byrd et al., 1994; Byrd, 1995; O'Connell et al., 2003; Thackray and Staley, 2017; see Table S1 in the Supplemental Material[1]). Based on topographic profiles obtained with a total station, Byrd (1995) determined the scarp height and converted it to the vertical separation following Bucknam and Anderson (1979) and Hanks and Andrews (1989). Altogether, 27 scarp profiles at 12 sites were analyzed by Byrd (1995, his table 3.1), with 11 profiles being located at Granite Canyon and only three profiles north of String Lake (Fig. 3). In the range center, vertical separation values varied between 25 and 30 m and decreased to 3 and 15 m in the southern part of the Teton fault (Byrd et al., 1994; Byrd, 1995). North of Leigh Lake, two profiles at Moran Bay and Coulter Canyon yielded vertical separations of 10 and 15.8 m, respectively (Fig. 3). In addition to the dip-slip movement, Byrd (1995) inferred 9 m and 26 m of lateral slip at two moraines located south of Taggart Lake and near Stewart Draw. Because more recent studies did not report a left-lateral slip component (Thackray and Staley, 2017; DuRoss et al., 2020, 2021; Zellman et al., 2020) and because we, too, did not find evidence of lateral slip at the sites of our scarp profiles, we will not consider this further in our study.

Based on high-resolution DEMs derived from lidar data that had become available in 2014, Thackray and Staley (2017) determined scarp heights from 16 topographic profiles between Moran Bay and Granite Canyon; i.e., their study was mostly restricted to the central section of the Teton fault (Fig. 3; Table S1). Arguing that the difference between scarp heights and vertical separation values is small and that the resulting vertical slip rates are indistinguishable, they used the scarp height as a proxy for the vertical slip. While this may be justified for the five shallow-dipping surfaces at Glacier Gulch, Taggart Lake, and Granite Canyon, the approach is problematic for the other studied landforms with a steeper far-field slope, including the lateral moraines at Taggart Lake, Bradley Lake, Glacier Gulch, and Granite Canyon and the scarp above String Lake. For the latter, Byrd (1995) showed that the large scarp height of 38 m reduces to a vertical separation of only 23 m due to high slope angles of 27° in the footwall and 14° in the hanging wall. Rather than attributing the along-strike variations in scarp height to the considerable variability in far-field slopes (cf. Byrd, 1995, his table 3.1), Thackray and Staley (2017) interpreted the variable scarp heights to result from differences in the age of the offset landforms. To calculate these ages, they used an average vertical slip rate of 0.82 ± 0.13 mm/yr, which they derived from the average scarp height of the five subhorizontal deglacial surfaces mentioned above, assuming an age of 14.7 ka for these landforms. Based on the additional assumption that this slip rate has been constant in space and time, they argued that the hillslope above String Lake and four lateral moraines are between 46 and 32 ka old. As an alternative interpretation to variations in landform ages, Thackray and Staley (2017) proposed that the offset landforms could be of similar (postglacial) age and that the strongly variable along-strike scarp heights reflect spatial variations in the rate of faulting. Arguing that the large scarp heights would have required very high offset rates, however, they did not favor this explanation. In a supplementary table, Thackray and Staley (2017) also provided vertical separation values (but no vertical slip) for their scarp profiles; however, their main conclusions and their postulated geomorphological ages were based on the scarp heights.

Additional scarp profiles were recently obtained at the sites of paleoseismological investigations (Fig. 3; Table S1) (DuRoss et al., 2020, 2021; Zellman et al., 2020). At the Buffalo Bowl trench, DuRoss et al. (2020) obtained a vertical separation of 6.2 m (range: 5.5–6.8 m) across the scarp with far-field slopes of 21° (footwall) and 16° (hanging wall). At the Leigh Lake trench site, scarp profiles across the three Teton fault strands yielded a total vertical separation of ≤7.2 m (Zellman et al., 2020). For two trenches across an uphill-facing scarp at Steamboat Mountain, DuRoss et al. (2021) reported vertical separation values of 2 and 3.9 m.

Besides the studies described above, the final report of the Jackson Lake Dam Minidoka Project included a diagram showing vertical offset rates for 17 sites along the Teton fault (O'Connell et al., 2003, their figure 2-7). Because no details on the site locations, scarp profiles, and age constraints are available, we will not consider this report further in our study. A simplified version of the figure from O'Connell et al. (2003) was later published without further details in Foster et al. (2010).

In summary, previous studies that analyzed scarp profiles across the Teton fault concentrated on <20 sites along its southern and central sections, with the consequence that the scarps north of Moran Bay as well as those around Phelps Lake and south of Granite Canyon (Fig. 3) remain poorly investigated. Furthermore, all previous studies assumed that vertical separation and/or scarp height are more or less an adequate approximation for the vertical slip and did not convert their values into vertical fault slip using the equations given above (cf. Caskey, 1995; Mackenzie and Elliott, 2017). With the high-resolution DEM based on lidar data acquired in 2014, it is now possible to analyze scarp profiles along the entire Teton fault and to determine the along-strike vertical slip distribution in much greater detail than before.

2.2 Constraints on the Postglacial Earthquake History of the Teton Fault

In order to resolve the postglacial earthquake history of the Teton fault and to better constrain its slip rate through time, trench excavations and sediment core analyses have been applied (Fig. 3). Trenching south of Phelps Lake (Granite Canyon) revealed two Holocene earthquakes at ca. 8 ka and 7–5 ka with a cumulative displacement of ~4 m (Byrd et al., 1994; Byrd, 1995). A trench at Buffalo Bowl near Teton Village, ~4 km south of the Granite Canyon trench site, revealed three surface-rupturing events at ca. 9.9 ka, ca. 7.1 ka, and

TABLE S1. SCARP HEIGHT AND VERTICAL SEPARATION ALONG THE TETON FAULT FROM PREVIOUS STUDIES

Location (offset landform if specified)	Scarp height (m)	Error of H (m)	Vertical separation (m)	Error of vs (m)	Reference
Northern fault section					
Steamboat Mountain trench sites A, B	2.0, 3.9	–	2.0, 4.0	0.3, 0.6	DuRoss et al. (2021, Fig. 9)
Coulter Canyon	17.5	–	15.8	–	Byrd (1995)
Central fault section					
Moran Bay	13.5	–	10	–	Byrd (1995)
Moran Bay	17.5	–	not determined	–	Thackray and Staley (2017)
Trapper Lake	62	–	26.9	–	Byrd (1995)
Leigh Lake trench sites (across three fault scarps)	–	–	sum 47.2	–	Zellman et al. (2020)
String Lake	37.9	–	22.8	–	Byrd (1995)
String Lake	38.0	3.0	23	1.4	Thackray and Staley (2017)
Southern shore of Jenny Lake	34.2	2.1	not determined	–	Thackray and Staley (2017)
Lupine Meadows	25	–	16	–	Byrd (1995)
Lupine Meadows	22.6	–	16.7	–	Byrd (1995)
Lupine Meadows	23.9	1.9	13.9	1.1	Thackray and Staley (2017)
Glacier Gulch (profile upstream of terminal moraine)	11.3	0.6	10.3	0.6	Thackray and Staley (2017)
Glacier Gulch (southern lateral moraine)	39.0	–	not determined	–	Thackray and Staley (2017)
Burned Wagon	16.0	–	9.7	–	Byrd (1995)
Burned Wagon	14.2	–	8.7	–	Byrd (1995)
Bradley Lake	16.5	–	13.4	–	Byrd (1995)
Bradley Lake	10.8	–	9	–	Byrd (1995)
Bradley Lake (northern lateral moraine)	14.7	1.2	3.3	0.3	Thackray and Staley (2017)
Bradley Lake (southern lateral moraine)	23.8	2.1	13.3	1.7	Thackray and Staley (2017)
Taggart Lake	20	–	15.9	–	Byrd (1995)
Taggart Lake	17.2	–	11.2	–	Byrd (1995)
Taggart Lake	20.6	–	14.7	–	Byrd (1995)
Taggart Lake (northern profile upstream of terminal moraine)	12.4	1.0	10.7	0.9	Thackray and Staley (2017)
Taggart Lake (northern profile upstream of terminal moraine)	11.2	0.9	10.5	0.8	Thackray and Staley (2017)
Taggart Lake (southern lateral moraine)	13.3	1.1	7.2	0.6	Thackray and Staley (2017)
Reeves Creek	12.0	–	8.9	–	Byrd (1995)
Hillslope south of Taggart Lake	21.4	1.7	6	0.6	Thackray and Staley (2017)

[1]Supplemental Material. Table S1 provides scarp height and/or vertical separation values determined by earlier studies. Figures S1–S4 show the scarp profiles sorted by the type of the displaced landforms. Please visit https://doi.org/10.1130/GEOS.S.14569359 to access the supplemental material, and contact editing@geosociety.org with any questions.

Downloaded from http://pubs.geoscienceworld.org/gsa/geosphere/article-pdf/doi/10.1130/GES02370.1/5364509/ges02370.pdf
by Technische Informationsbibliothek (TIB) user

ca. 4.6 ka, which produced a cumulative vertical separation of 6.3 ± 0.5 m as derived from marker horizons dipping 13°–21° on both trench walls (DuRoss et al., 2020). By dividing the cumulative vertical separation by the number of events found in the trench, the slip per event was estimated to be 2.1 ± 0.4 m (DuRoss et al., 2020). In addition to the information on the paleoearthquakes, radiocarbon and optically stimulated luminescence (OSL) ages from the Buffalo Bowl trench constrained the age of the hillslope deposits and hence the age of the fault scarp. The age data indicate that the ~3-m-thick alluvial fan and slope colluvium sediments were deposited between ca. 15 and ca. 10.5 ka (DuRoss et al., 2020) and afterwards offset by the Teton fault.

In the central section of the Teton fault, trenches across two of three strands above Leigh Lake (Fig. 3) revealed two earthquakes at ca. 10 ka and ca. 6 ka with displacements of 0.4–1.7 m and 1.1–1.7 m, respectively (Zellman et al., 2020). In the northernmost part of the Teton fault, two trenches across an uphill-facing scarp at Steamboat Mountain provided evidence for two earthquakes at 9.7 ± 0.9 ka and 5.5 ± 0.2 ka, respectively (Fig. 3) (DuRoss et al., 2021). The cumulative vertical displacement caused by the two events is 4.0 ± 0.5 m (2.0 ± 0.6 and 2.0 ± 1.0 m for the most recent event and the penultimate event, respectively). The ~2-m-thick postglacial sedimentary succession east of the uphill-facing scarp (i.e., in the fault hanging wall) formed between ca. 12 and ca. 2 ka, as shown by ^{14}C and OSL ages (DuRoss et al., 2021).

In contrast to the paleoseismological studies, which captured only the Holocene earthquake history of the Teton fault, sediment cores from Jenny Lake cover the earthquake history since the onset of sedimentation in the lake at ca. 14 ka, i.e., after the melting of the Pinedale valley glaciers (Fig. 3) (Larsen et al., 2016, 2019). Seven major earthquakes between ca. 14 and 7.7 ka are recorded by turbidite deposits each having a thickness of up to ~39 cm, while two other events at 13.3 ka and 5.3 ka are associated with turbidite layers, which are each 2–3 cm thick (Larsen et al., 2019). Given that the ca. 10 ka and ca. 5.3 ka events have also been identified in the paleoseismological trenches (Byrd et al., 1994; DuRoss et al., 2020, 2021; Zellman et al., 2020), this provides strong evidence that these earthquakes ruptured the entire Teton fault. Apart from the lake sediments, Larsen et al. (2019) also obtained ^{10}Be exposure ages from boulders that were deposited by a landslide, which initiated on the northern flank of the Cascade Canyon mouth and transported coarse material into Jenny Lake. Three boulders from the northern landslide yielded a mean ^{10}Be age of 14.0 ± 0.2 ka, which coincides with the age of the oldest turbidite deposit of 14.0 ± 0.44 ka and indicates that the landslide was most likely triggered by the earthquake (Larsen et al., 2019).

3. DATA AND METHODS

3.1 Digital Elevation Models Used for Fault Scarp Profiles

To determine the vertical displacement along strike of the Teton normal fault, topographic profiles across the fault scarp were constructed from a 1-m-resolution DEM processed from lidar data acquired in 2014. The northern part of the DEM covering the Grand Teton National Park is available through the U.S. Geological Survey National Map website (https://www.usgs.gov/core-science-systems/national-geospatial-program/national-map; accessed February 2020). For the area south of the Grand Teton National Park, lidar data were obtained from the Teton County Conservation District and processed into a 1-m-resolution DEM by M.S. Zellman (Zellman et al., 2019).

3.1 Vertical Slip from Topographic Profiles across Tectonically Offset Geomorphic Features

From the DEM, we extracted topographic profiles using the following criteria: Profiles (1) are oriented perpendicular to the fault scarp, (2) are located at well-defined landforms such as river terraces, moraines, or alluvial fans, and (3) extend over a distance of at least 100 m. The sites for the scarp profiles across offset river terraces were carefully chosen to be located in areas where sediment deposition in the hanging wall (or the fault footwall) was negligible. The profiles were drawn as line features in GlobalMapper software and exported to Generic Mapping Tools (Wessel et al., 2013) for plotting. To preserve the angular relations, all profiles were plotted without vertical exaggeration and straight lines were visually fitted to both the footwall and hanging-wall surfaces (cf. Bucknam and Anderson, 1979).

Depending on the far-field slope angles of the fault hanging wall and footwall as well as on the difference between them, we classified the profiles into four quality categories and pursued different approaches to determine the vertical separation Δz. High-quality category I profiles have a slope of ≤5° in both the footwall and hanging wall. Profiles in category II have a slope of >5° in the footwall or hanging wall but the difference in slope is ≤5°. For category I and II profiles, we determined the vertical separation Δz in the middle of the fault scarp (Fig. 4A) and converted this value to two values for the vertical slip S_z by using the slopes of the hanging wall and footwall, respectively. By taking the mean of the two S_z values, we estimated the vertical fault slip and its uncertainty, which also accounts for the range of permissible dips of the lines used to determine the vertical separation. Category III profiles show slopes of >5° in the footwall and hanging wall and a difference that is >5° but <10°. In category IV profiles, the slope in both the footwall and hanging wall is >5° and differs by >10°. For category III and IV profiles, we determined minimum and maximum values for Δz at the toe and crest of the scarp, respectively (Fig. 4B). We then converted Δz_{min} and Δz_{max} to values of S_{z_min} and S_{z_max} using the far-field slope in the hanging wall and footwall, respectively. All conversions from Δz to S_z were performed assuming a dip of 60° for the Teton fault, which represents an average value within the range of 45°–75° given by Byrd et al. (1994).

Some scarp profiles show a secondary fault, which can be either synthetic or antithetic (the latter results in a graben structure in the hanging wall). In both cases, we determined the vertical slip associated with the secondary fault in the way described above. For synthetic secondary faults, we added the obtained

Downloaded from http://pubs.geoscienceworld.org/gsa/geosphere/article-pdf/doi/10.1130/GES02370.1/5364509/ges02370.pdf
by Technische Informationsbibliothek (TIB) user

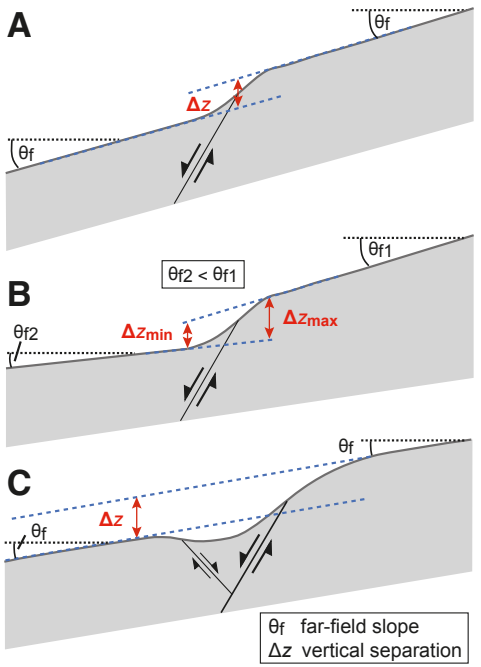

Figure 4. Sketches illustrating the determination of the vertical separation Δ*z* for scarps with similar far-field slopes θ_f in the footwall and hanging wall (A), scarps with different slopes in the footwall and hanging wall (B), and scarps in presence of a graben structure and similar slopes in footwall and hanging wall (C). After Caskey (1995).

S_z value to the vertical slip derived for the main fault. In presence of a graben, the S_z value obtained for the antithetic secondary fault was subtracted from the vertical slip of the main fault (cf. Caskey, 1995; McCalpin, 2009). In one case (profile Pm1), the far-field slopes of the hanging wall and footwall were equal, and we applied the approach depicted in Figure 4C to determine the vertical separation (cf. Caskey, 1995).

4. RESULTS

We extracted a total of 54 scarp profiles from the DEM (Table 1; Fig. 5). To distinguish the different kinds of offset geomorphological features, we divided the scarp profiles into four groups: Pm, Pg, Pc, and Pf, which refer to profiles that offset moraines, glacial surfaces (bedrock or bedrock with a thin sediment cover), hillslope colluvium, and fluvial or fluvially reworked glacial deposits, respectively. Altogether, seven profiles from offset lateral and recessional moraines, 11 profiles across offset glacial surfaces, 23 profiles from offset hillslope colluvium, and 13 profiles from offset fluvial or fluvially reworked glacial deposits were used (Table 1). Far-field slopes in the fault footwall and hanging wall range from 0° to 30° (Supplemental Figs. S1–S4 [footnote 1]). In total, 35 profiles fall into category I and II and 19 profiles fall into category III and IV (Table 1). This implies that we were able to derive a mean S_z value from about two-thirds of all scarp profiles, while the remaining one third yielded ranges from S_{z_min} to S_{z_max} due to relatively large differences in slope between footwall and hanging wall. The latter was the case for most profiles along offset moraine crests (profiles Pm2, Pm4–7) and for most Pc profiles from the southern part of the Teton fault south of Jenny Lake. Generally, vertical separations north of Jenny Lake are constrained by mostly category I and II profiles, whereas the quality of profiles in the southern part is mixed, with offset lateral and recessional moraine crests yielding category III and IV profiles and fluvial terraces yielding category I and II profiles.

Figure 5 shows the scarp profiles together with their location maps grouped by regions along the Teton fault (in Figs. S1–S4 [footnote 1], the profiles are shown sorted by the type of the displaced landforms). From north to south along the fault, the first group of three profiles is located at the northeastern shore of Jackson Lake and provides the vertical slip S_z from two downhill-facing scarps (profile Pg1: 5.2 ± 0.3 m; Pg2: 6.7 ± 0.3 m) and one uphill-facing scarp (Pc1: 6.5–9.3 m). Along the northwestern shore of Jackson Lake, profiles Pg3–Pg5 are located where the Teton fault offsets bedrock surfaces with macroscale glacial striations and yield S_z values of 7.8–15.4 m (Fig. 5). Two other profiles across offset glacial surfaces are located further south (profile Pg6: 16.3 ± 1.6 m; Pg7: 23.9 ± 2.4 m). In addition, six profiles from scarps across hillslope colluvium (profiles Pc2–Pc7) and two profiles from offset fluvial deposits at valley exits (Pf1, Pf2) were obtained along the western shore of Jackson Lake. Between the southern end of Jackson Lake and Jenny Lake, where the scarp reaches its greatest height and is particularly well preserved, we derived the vertical slip from profiles across offset glacial features (profiles Pg8–Pg10), hillslope colluvium near Trapper Lake (Pc8), Leigh Lake (Pc9–Pc11), and String Lake (Pc12–Pc16), as well as a moraine ridge north of Jenny Lake (Pm1). Note that we analyzed several profiles near String Lake because at this well-known site in the range center, the far-field slope varies laterally and antithetic faults occur locally (Fig. 5). South of Jenny Lake, at the location of profile Pc17, the Teton fault scarp is well expressed but the slopes in the footwall and hanging wall differ greatly, leading to a large S_z range of 8.7–36.5 m. From Glacier Gulch to the southern end of the Teton fault, six profiles from offset moraines (profiles Pm2–Pm7), one profile across an offset glacial surface (Pg11), six profiles with offset hillslope colluvium (Pc18–Pc23), and 11 profiles from displaced fluvial deposits (Pf3–Pf13) could be derived. Importantly, we were able to obtain vertical slip values at sites where the Teton fault offsets both lateral moraines and fluvial deposits at the exit of the same valley (Fig. 6; Avalanche Canyon at Taggart Lake: profiles Pm2, Pf6; Granite Canyon: Pm4–Pm5, Pf9–Pf10), which allows us to constrain the relative timing of scarp formation. Near

Downloaded from http://pubs.geoscienceworld.org/gsa/geosphere/article-pdf/doi/10.1130/GES02370.1/5364509/ges02370.pdf
by Technische Informationsbibliothek (TIB) user

TABLE 1. TECTONICALLY OFFSET GEOMORPHOLOGIC FEATURES USED FOR DERIVING VERTICAL SLIP FROM SCARP PROFILES ACROSS THE TETON FAULT

Profile	Coordinates at scarp base (°W, °N)	Elevation at scarp base (m)	Category*	Δz or Δz_{min}; Δz_{max} (m)	Δz_2 or Δz_{2min}; Δz_{2max} (m)	S_z ± error (m)	S_{z_min} (m)	S_{z_max} (m)	Remarks
Lateral moraines									
Pm1	110.74479, 43.77544	2318	II	22.8	–	26.6 ± 2.7	–	–	Lateral moraine; north of Jenny Lake
Pm2	110.76246, 43.71170	2241	III	27.9; 37.8	10.5	–	17.5	31.0	Lateral moraine with graben; north of Taggart Lake
Pm3	110.78708, 43.67051	2341	II	16.7	3.0	14.6 ± 1.5	–	–	Recessional moraine with graben; north of Phelps Lake
Pm4	110.81163, 43.62169	2071	III	9.1	1.5; 2.3	–	11.7	15.0	Lateral moraine with two fault scarps; north of Granite Canyon
Pm5	110.81444, 43.61101	2027	III	9.9; 14.0	–	–	10.1	15.5	Lateral moraine with two fault scarps; south of Granite Canyon
Pm6	110.85884, 43.56527	2096	III	8.4; 15.5	–	–	9.7	20.5	Lateral moraine north of Pm7; valley north of Jensen Canyon
Pm7	110.85940, 43.56378	2067	III	8.7; 16.1	–	–	10.6	21.7	Lateral moraine south of Pm6; valley north of Jensen Canyon
Glacial surfaces									
Pg1	110.69701, 44.03980	2249	I	5.2	–	5.2 ± 0.3	–	–	Uphill-facing scarp across sediment-covered surface with glacial striations; channel at scarp base; eastern shore of Jackson Lake
Pg2	110.69779, 44.03640	2239	I	6.6	–	6.7 ± 0.3	–	–	Sediment-covered surface with glacial striations; channel at scarp base; eastern shore of Jackson Lake
Pg3	110.70187, 43.98192	2101	III	7.2; 11.9	–	–	7.8	14.1	Surface with macroscale striations; western shore of Jackson Lake
Pg4	110.70216, 43.98148	2112	II	11.8	–	13.9 ± 1.4	–	–	Surface with macroscale striations; western shore of Jackson Lake
Pg5	110.70192, 43.98005	2117	I	14.8	–	15.4 ± 0.8	–	–	Surface with macroscale striations; western shore of Jackson Lake
Pg6	110.70571, 43.95126	2157	II	15.3	–	16.3 ± 1.6	–	–	Rough glacial surface; western shore of Jackson Lake
Pg7	110.72791, 43.89497	2140	II	22.0	–	23.9 ± 2.4	–	–	Glacial depositional surface; western shore of Jackson Lake
Pg8	110.74823, 43.85041	2271	II	21.9	–	23.6 ± 2.4	–	–	Rough glacial surface; north of Trapper Lake
Pg9	110.73608, 43.84059	2175	II	21.0	–	23.7 ± 2.4	–	–	Glacial depositional surface; near Trapper Lake
Pg10	110.73605, 43.84041	2175	II	21.6	–	24.1 ± 2.4	–	–	Glacial depositional surface; near Trapper Lake
Pg11	110.80798, 43.63627	2154	II	9.9	–	10.4 ± 1.0	–	–	Small offset ridge of basal moraine; south of Phelps Lake
Hillslope colluvium									
Pc1	110.70078, 44.02952	2137	III	8.7; 11.6	–	–	6.5	9.3	Uphill-facing scarp; eastern shore of Jackson Lake
Pc2	110.70403, 43.97632	2141	II	13.2	–	15.2 ± 1.5	–	–	Moran Bay; western shore of Jackson Lake
Pc3	110.70413, 43.97628	2144	II	11.8	–	13.7 ± 1.4	–	–	Western shore of Jackson Lake
Pc4	110.71029, 43.92509	2121	III	12.1; 16.7	2.4	–	10.0	15.8	With graben; offset is a minimum value because of second minor fault strand east of profile; western shore of Jackson Lake
Pc5	110.72428, 43.91109	2152	II	14.8	–	15.9 ± 1.6	–	–	At transition between hillslope colluvium and alluvial fan
Pc6	110.72474, 43.89980	2121	II	12.3	–	13.5 ± 1.4	–	–	Hillslope colluvium in footwall; glacial depositional surface in hanging wall; western shore of Jackson Lake
Pc7	110.73136, 43.89038	2167	II	11.3	–	12.8 ± 1.3	–	–	Possibly minimum value because fault strike changes with a decrease in scarp height south of profile location; western shore of Jackson Lake
Pc8	110.73609, 43.83388	2160	II	19.5	–	25.1 ± 2.5	–	–	Footwall and hanging wall with similar topographic signature; between Jackson Lake and Leigh Lake
Pc9	110.73536, 43.79847	2106	I	25.0	5.9	19.0 ± 1.0	–	–	With graben; offset channel bed at southern terminal moraines of Yellowstone ice cap; south of Leigh Lake
Pc10	110.73558, 43.79825	2105	I	22.9	3.4	20.7 ± 1.0	–	–	With graben; offset channel bed at southern terminal moraines of Yellowstone ice cap; south of Leigh Lake

(*continued*)

Downloaded from http://pubs.geoscienceworld.org/gsa/geosphere/article-pdf/doi/10.1130/GES02370.1/5364509/ges02370.pdf
by Technische Informationsbibliothek (TIB) user

TABLE 1. TECTONICALLY OFFSET GEOMORPHOLOGIC FEATURES USED FOR DERIVING VERTICAL SLIP FROM SCARP PROFILES ACROSS THE TETON FAULT (*continued*)

Profile	Coordinates at scarp base (°W, °N)	Elevation at scarp base (m)	Category*	Δz or Δz_{min}; Δz_{max} (m)	Δz_2 or Δz_{2min}; Δz_{2max} (m)	S_z ± error (m)	S_{z_min} (m)	S_{z_max} (m)	Remarks
Hillslope colluvium (*continued*)									
Pc11	110.73572, 43.79812	2105	I	21.6	1.4	21.1 ± 1.1	–	–	With graben; offset channel bed at southern terminal moraines of Yellowstone ice cap; south of Leigh Lake
Pc12	110.73902, 43.79279	2158	III	26.2	6.0	25.3 ± 2.5	–	–	With graben; at String Lake
Pc13	110.73927, 43.79249	2168	IV	16.5; 29.9	5.6	–	12.5	32.7	With graben; at String Lake
Pc14	110.73949, 43.79164	2181	IV	19.6; 32.0	1.0	–	20.9	38.9	With graben; at String Lake
Pc15	110.74011, 43.79126	2202	III	15.1; 24.7	1.7	–	15.6	29.8	With graben; at String Lake
Pc16	110.74044, 43.79100	2212	III	15.8; 24.9	2.5	–	16.3	30.8	With graben; at String Lake
Pc17	110.74567, 43.74608	2110	IV	8.1; 26.2	–	–	8.7	36.5	South of Jenny Lake
Pc18	110.76104, 43.69759	2119	IV	11.1; 15.8	–	–	11.8	18.9	At transition between hillslope colluvium and alluvial deposits; south of Taggart Lake
Pc19	110.76509, 43.68639	2181	IV	6.3; 15.3	–	–	7.1	20.6	South of Taggart Lake
Pc20	110.84261, 43.58745	2069	II	6.2	–	7.8 ± 0.8	–	–	Buffalo Bowl trench site
Pc21	110.84276, 43.58732	2071	II	5.1	–	6.3 ± 0.6	–	–	Buffalo Bowl trench site
Pc22	110.85298, 43.57869	2142	III	9.4; 14.1	–	–	11.0	18.5	Between Buffalo Bowl trench site and Jensen Canyon
Pc23	110.8596, 43.56803	2068	II	6.5	–	8.6 ± 0.9	–	–	Between Buffalo Bowl trench site and Jensen Canyon
Fluvial deposits and reworked glacial material									
Pf1	110.72009, 43.91544	2214	II	18.3	–	21.1 ± 2.1	–	–	Small terrace in alluvial fan; western shore of Jackson Lake
Pf2	110.75530, 43.86803	2092	I	15.4	–	16.0 ± 0.8	–	–	Flat rough surface at valley exit toward Jackson Lake
Pf3	110.74892, 43.73756	2140	II	17.9	1.7	19.1 ± 1.9	–	–	Terrace in alluvial fan; south of Jenny Lake
Pf4	110.75242, 43.72940	2143	I	10.8	–	11.0 ± 0.6	–	–	Flat rough surface (basal moraine) at Glacier Gulch valley exit between lateral moraines, west of recessional moraine sequence
Pf5	110.75286, 43.72849	2144	I	7.0	–	7.3 ± 0.4	–	–	Flat rough surface (basal moraine) at Glacier Gulch valley exit between lateral moraines, west of recessional moraine sequence
Pf6	110.76245, 43.70765	2107	I	11.7	–	12.0 ± 0.6	–	–	Flat surface at valley exit between lateral moraines, upstream of terminal moraines; Taggart Lake
Pf7	110.76544, 43.68440	2160	II	6.9	–	7.8 ± 0.8	–	–	River terrace at valley exit; between Taggart and Phelps Lake
Pf8	110.80425, 43.65246	2025	I	8.5	–	8.6 ± 0.4	–	–	Flat surface at valley exit between lateral moraines upstream of terminal moraines; Phelps Lake
Pf9	110.81104, 43.61853	1988	I	12.1	1.5	10.9 ± 0.5	–	–	Flat surface in moraine material at valley exit upstream of terminal moraines; north of Granite Creek; Granite Canyon
Pf10	110.81241, 43.61362	1981	I	11.8	–	11.9 ± 0.6	–	–	Flat surface in moraine material at valley exit upstream of terminal moraines; south of Granite Creek; Granite Canyon
Pf11	110.84745, 43.58244	2086	III	4.8; 8.7	–	–	5.5	10.9	Narrow terrace in alluvial fan; south of Buffalo Bowl trench site
Pf12	110.85521, 43.57080	2046	II	12.2	2.1	12.0 ± 1.2	–	–	Alluvial fan; between Buffalo Bowl trench site and Jensen Canyon
Pf13	110.85967, 43.55872	2003	III	4.5; 6.2	–	–	4.9	7.2	Alluvial fan; between Buffalo Bowl trench site and Jensen Canyon

*Category I—slope in footwall and hanging wall ≤5°; category II—slope in footwall and hanging wall >5° and difference in slope ≤5°; category III—slope in footwall and hanging wall >5° and difference in slope >5° and <10°; category IV—slope in footwall and hanging wall >5° and difference in slope >10°.

Note: Dash indicates that the determination of this value does not apply to the respective profile. Error was estimated from the mean of the S_z values in the footwall and hanging wall, taking into account the range of permissible dips of the lines used to determine the vertical separation.

Downloaded from http://pubs.geoscienceworld.org/gsa/geosphere/article-pdf/doi/10.1130/GES02370.1/5364509/ges02370.pdf
by Technische Informationsbibliothek (TIB) user

Figure 5 is interactive. Place the mouse cursor over the names or color-filled circles of the scarp profiles in A to view the related scarp profiles and detailed location maps in B. To interact with Figure 5 if reading the full-text version of this paper, please visit https://doi.org/10.1130/GEOS.S.14998629.

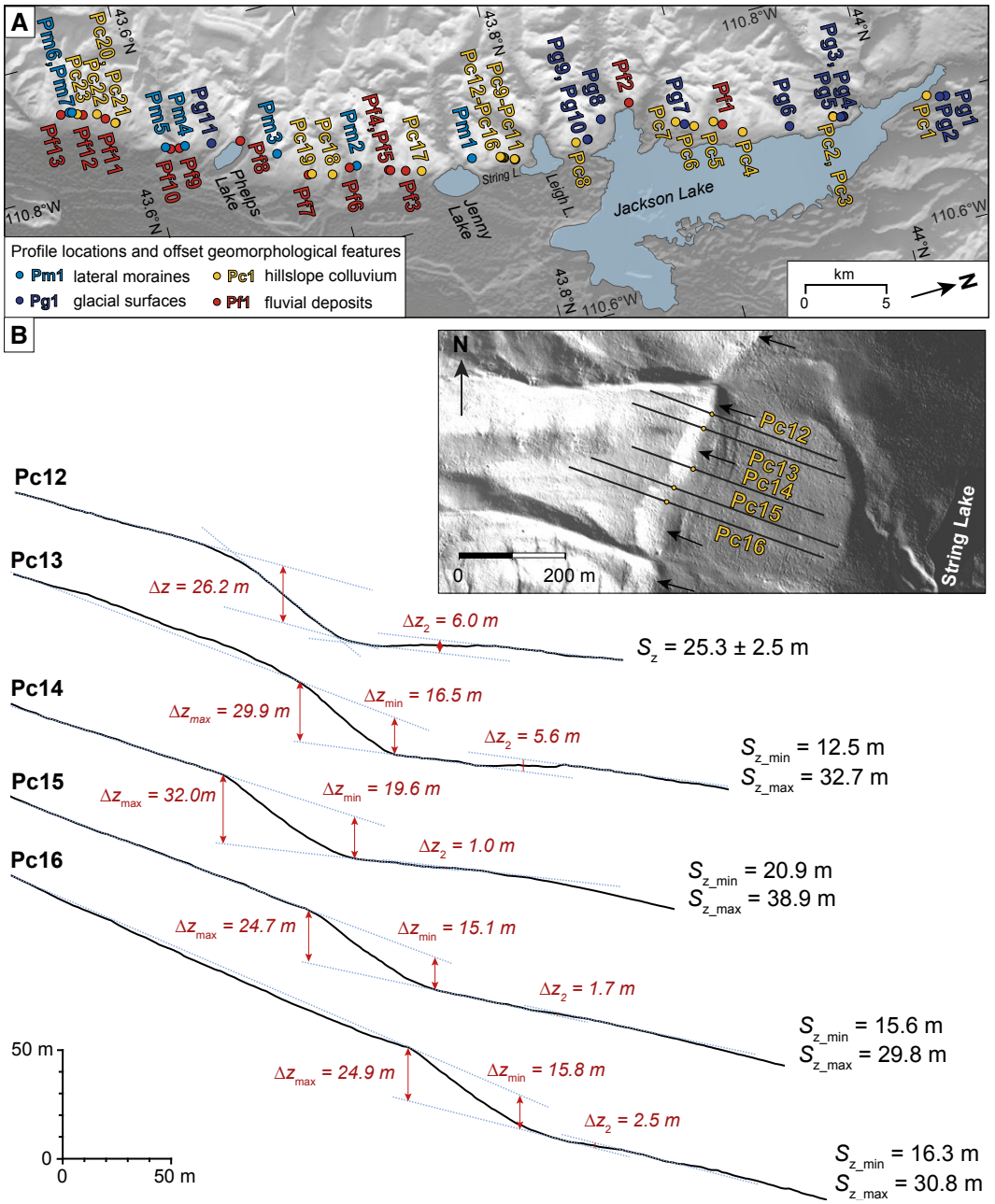

Figure 5 (interactive). Determination of the vertical separation Δz and vertical slip S_z from topographic profiles across scarps of the Teton fault. (A) Location map showing names and locations (color-filled circles) of the scarp profiles. (B) Profiles and their detailed location maps. The colored dot in the middle of each profile line represents the base of the scarp (Table 1). Arrows (black or white) indicate the surface trace of the Teton fault. Figures S1–S4 (see text footnote 1) show the profiles grouped by the type of offset geomorphological feature. Note for viewing: Please place the mouse cursor over the names or color-filled circles of the scarp profiles in A to view the related scarp profiles and detailed location maps in B. To interact with Figure 5 if reading the full-text version of this paper, please visit https://doi.org/10.1130/GEOS.S.14998629.

Downloaded from http://pubs.geoscienceworld.org/gsa/geosphere/article-pdf/doi/10.1130/GES02370.1/5364509/ges02370.pdf
by Technische Informationsbibliothek (TIB) user

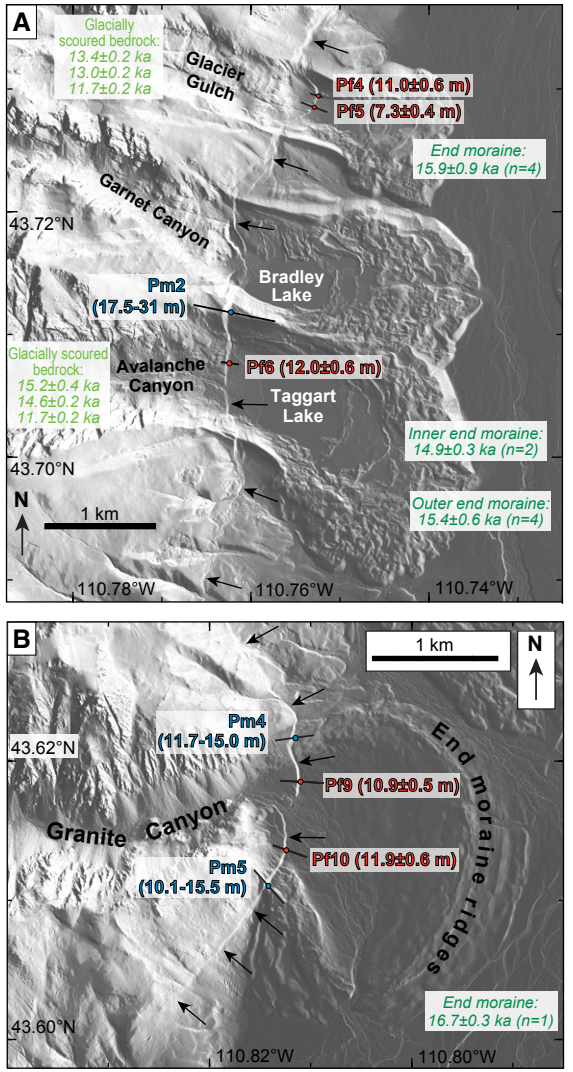

Figure 6. Two detail maps (for location, see Fig. 3) illustrating the spatial relationship between Pinedale moraines and younger fluvial terraces, which formed after the retreat of the valley glaciers. Scarp profiles (labeled in blue and red) are shown together with vertical slip derived from the respective offset landform. ^{10}Be exposure ages from moraines (dark green) and glacially scoured bedrock (light green) are from Pierce et al. (2018); *n* indicates the number of dated boulders. Scarp of the Teton normal fault is marked by black arrows. (A) Area of Taggart Lake, Bradley Lake, and Glacier Gulch, where end moraines marked by irregular lobate ridges encircle the canyon mouths. Note that we did not use lateral moraines other than at profile Pm2 because they yielded scarp profiles of low quality. (B) Granite Canyon area with moraine ridges around the canyon mouth.

the Buffalo Bowl trench site (DuRoss et al., 2020), two profiles across offset hillslope colluvium yield vertical slip values of 7.8 ± 0.8 m (profile Pc20) and 6.3 ± 0.6 m (Pc21). In summary, our results show a general increase in vertical slip from the southern and northern ends of the Teton fault toward its central part, a finding that we will discuss in the next section.

5. DISCUSSION

5.1 Vertical Slip Distribution along Strike of the Teton Normal Fault

Figure 7 shows the location map of the scarp profiles together with a diagram in which the vertical slip S_z derived from the scarp profiles is plotted against the distance along strike of the Teton fault. Color-filled circles with error bars are related to category I and II profiles, for which the vertical slip was derived as a mean value, with the uncertainty reflecting the upper and lower bounds of possible S_z values derived from the respective scarp profile; colored vertical bars represent category III and IV profiles, from which the vertical displacement was derived as a range between S_{z_min} and S_{z_max} indicated by the bar height. The diagram in Figure 7B reveals that the vertical slip is highest (27–23 m) between Jenny Lake and Trapper Lake. The slip distribution is characterized by a pronounced asymmetry because the vertical slip remains high (>20 m) for a distance of ~15 km north of Jenny Lake, whereas it decreases to <20 m within 7 km south of Jenny Lake. To visualize this asymmetry, we included a gray curve in Figure 7B, which we calculated as a spline function using the data points with the highest vertical displacements, giving more weight to category I and II than to category III and IV profiles. This curve highlights that the northern part of the Teton fault (north of Jenny Lake) has accrued more slip than the southern part (south of Jenny Lake). In the northern part of the fault, where the S_z values from glacial landforms are constrained by mostly category I and II profiles, the gray curve resembles an ideal fault displacement profile, with slip gradually decreasing toward the northern fault tip. A gradual decrease in slip is also observable from Jenny Lake to the south; however, the displacement profile is less well constrained compared to the northern part because the moraines (profiles Pm4–Pm7) yielded category III and IV profiles and hence only S_{z_min} to S_{z_max} ranges.

A comparison between the gray curve and the curves determined for the different landform groups (Fig. 7B) reveals that the shape of the former mainly reflects the S_z values derived from moraines and glacial surfaces, whereas the curves for the Pc and Pf profiles are located below it. This pattern illustrates that the offset lateral moraines and glacial surfaces generally show higher S_z values compared to the other landforms. Scarps across hillslope colluvium (Pc profiles) have recorded a wider range of vertical slip values, which generally vary between the values obtained from offset glacial features and those from offset fluvial deposits (Fig. 7B). The overall slip distribution recorded by the Pc profiles is asymmetric with respect to the range center, with the maximum slip (19–25 m) occurring between Jenny Lake and Trapper Lake. Finally, the

Downloaded from http://pubs.geoscienceworld.org/gsa/geosphere/article-pdf/doi/10.1130/GES02370.1/5364509/ges02370.pdf
by Technische Informationsbibliothek (TIB) user

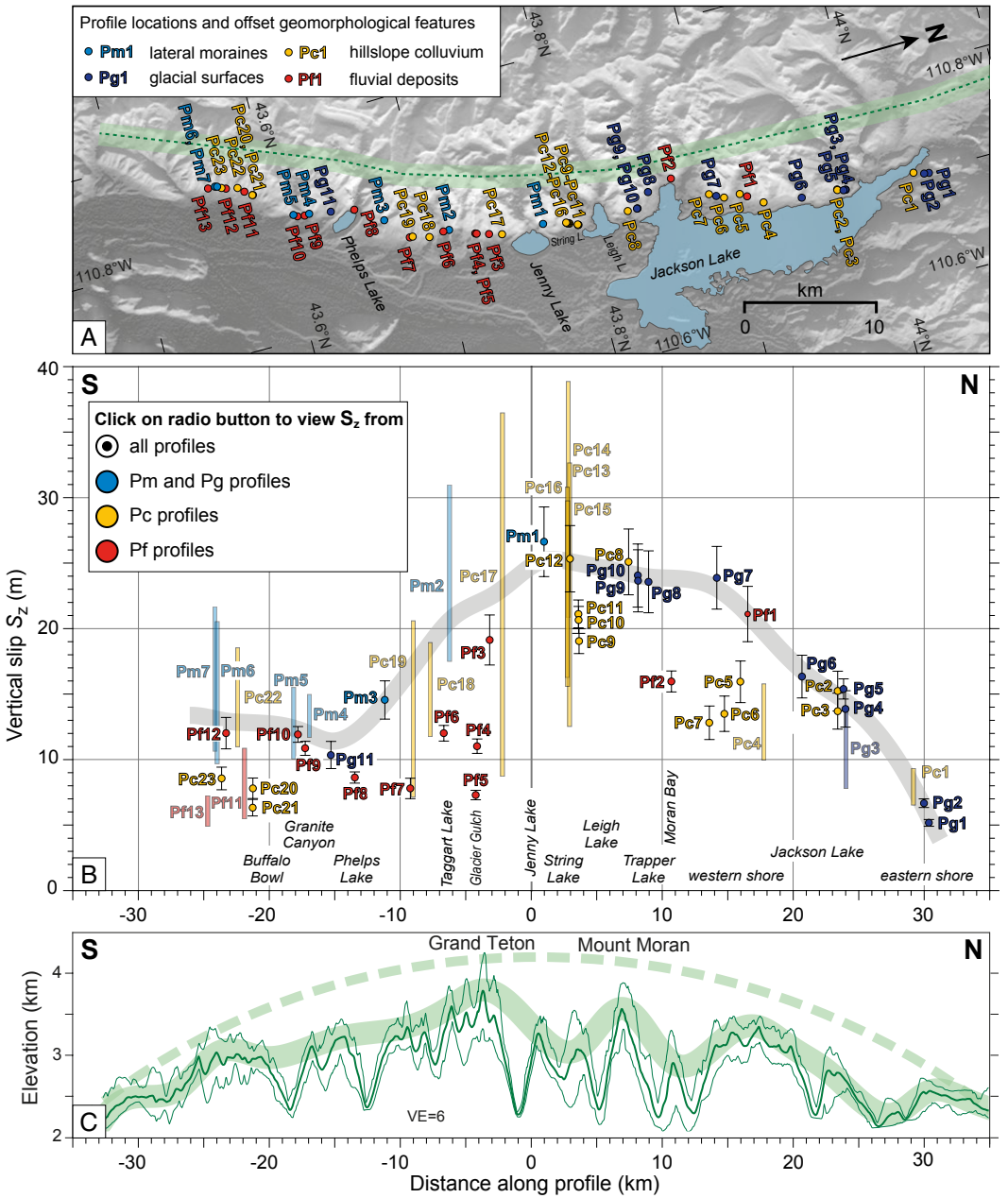

Figure 7B is interactive. Use the radio buttons in the legend to view the S_z values from all profiles (gray curve through data points with highest vertical slip) or separately from the different groups (blue, yellow, and red curves, respectively). To interact with Figure 7B if reading the full-text version of this paper, please visit https://doi.org/10.1130/GEOS.S.14998629.

Figure 7. Vertical slip distribution along strike of the Teton normal fault. (A) Location map of scarp profiles (color-filled circles) and swath profile shown in C (in green). (B) (interactive) Diagram showing vertical fault slip S_z versus distance along the Teton normal fault. Note that we placed the zero distance value at Jenny Lake at the mouth of Cascade Canyon. Color-filled circles with error bars are related to category I and II profiles, for which the vertical displacement was derived as a mean value. Color-filled circles with error bars are related to category I and II profiles, for which the vertical slip was derived as a mean value, with the uncertainty reflecting the upper and lower bounds of possible S_z values derived from the respective scarp profile. Colored vertical bars represent category III and IV profiles, from which the vertical displacement was derived as a range between $S_{z\ min}$ and $S_{z\ max}$ indicated by the bar height. Please use the radio buttons in the legend to view the S_z values from all profiles (gray curve through data points with highest vertical slip) or separately from the different groups (blue, yellow, and red curves, respectively). To interact with Figure 7B if reading the full-text version of this paper, please visit https://doi.org/10.1130/GEOS.S.14998629. (C) Swath profile (width: 2 km) along the crest of the Teton Range. Vertical exaggeration (VE) is 6×. The dark green lines represent the mean (thick line) and the maximum and minimum elevation values (thin lines above and below the thick line, respectively) along the swath profile. Thick green line indicates an envelope along the peaks of the Teton Range; dashed green line shows a symmetric parabolic curve for comparison.

Downloaded from http://pubs.geoscienceworld.org/gsa/geosphere/article-pdf/doi/10.1130/GES02370.1/5364509/ges02370.pdf
by Technische Informationsbibliothek (TIB) user

Pf profiles show S_z values of 6–12 m between the southern end of the fault and Glacier Gulch (Fig. 7B). At Granite Canyon, Glacier Gulch, and Avalanche Canyon, Pf profiles yield lower slip values than the Pm profiles across offset lateral moraines (Fig. 6), which was also noted by Byrd (1995) and Thackray and Staley (2017). For the Pf profiles with subhorizontal surfaces (e.g., Pf4, Pf6, Pf9–Pf10), our vertical slip values are similar to the scarp height and vertical separation values reported by Thackray and Staley (2017) for these sites. This is not surprising because the difference between scarp height, vertical separation, and vertical slip becomes small for far-field slopes of <5° (cf. Fig. 2). North of Glacier Gulch, our Pf profiles show higher slip values, as illustrated by the red curve in Figure 7B.

5.2 Constraints on the Ages of Landforms and Offsets Recorded by the Teton Fault Scarps

As described in Section 5.1, scarp profiles from offset lateral and recessional moraines (Pm profiles) and glacial surfaces (Pg) yield higher slip values than profiles across offset fluvial features (Pf) and most hillslope colluvium (Pc). Given that geomorphological investigations, reconstructions of the LGM ice extent, and ^{10}Be exposure ages indicate that the moraine systems around the mouths of the Teton Range valleys formed during the Pinedale glaciation (Fig. 3) (Love et al., 2003; Licciardi and Pierce, 2008, 2018; Pierce et al., 2018), the vertical slip recorded by the Teton fault scarps is of postglacial age. This also applies to the offset lateral moraines, which may be slightly older than the terminal moraines as indicated by a preliminary mean ^{10}Be age of 19.4 ± 1.7 ka (based on two boulders) from Phelps Lake (Fig. 3) but still formed during the LGM (Pierce et al., 2018). Our interpretation is also supported by the observation that the offset glacial features consistently show the highest vertical slip and together form an approximately parabolic displacement profile. The tapering of slip toward the northern fault end into previously glaciated terrain further indicates that the macroscale striations, which are visible in the DEM along the western and northeastern shores of Jackson Lake (Fig. 5), formed during the last glaciation and were offset by post-Pinedale earthquakes. This interpretation is supported by the age constraints from the Steamboat Mountain trenches (DuRoss et al., 2021).

The observation that the Pc profiles generally yield S_z values equal to or lower than those of the Pm and Pg profiles (Fig. 7B) indicates that the hillslope colluvium at String Lake and other sites did not form before the LGM, in contrast to the inference of Thackray and Staley (2017). For profiles Pc20 and Pc21, the postglacial age of the colluvial and alluvial sediments is confirmed by ^{14}C and OSL ages from the Buffalo Bowl trench (DuRoss et al., 2020). Although this is the only site where the hillslope colluvium has been dated, we regard it as unlikely that the colluvium is generally older than the LGM moraines and glacial surfaces for the following reasons. First, while the present-day hillslopes along the Teton Range front are largely forested and may be relatively stable, it is highly unlikely that a similar vegetation existed during the LGM, when climate conditions were drier and much cooler and valley glaciers and an ice cap as much as 1 km thick covered the Teton-Yellowstone region. The abundance of clastic glacial sediment lacking organic matter from soils and terrestrial plants in the lowermost sediment unit of Jenny Lake indicates that there was little soil development or vegetation in the Cascade Canyon catchment between 14 ka and 11.5 ka (Larsen et al., 2016). The Jenny Lake sediment record indicates recolonization of the Teton Range by vegetation only after ca. 11.5 ka (Larsen et al., 2016). Glacial sediments devoid of organic matter also occur at the Leigh Lake trench site, where subglacial diamicton without organic matter yielded OSL ages of 11.5–9.5 ka (Zellman et al., 2020). In contrast, the overlying scarp-derived colluvium contains organic matter and thus could be dated by ^{14}C dating, which indicated an age of 7.7 ka or younger (Zellman et al., 2020).

Compared to Pm and Pg profiles, Pf profiles across fluvial deposits yield lower vertical slip (Fig. 7B), which we interpret to reflect a younger age for their formation relative to the glacial landforms. The age difference is particularly clear for the flat surfaces that formed in fluvially reworked glacial deposits upstream of Pinedale terminal and recessional moraines at Glacier Gulch (profiles Pf4, Pf5), Taggart Lake (Pf6), Phelps Lake (Pf8), and Granite Canyon (Pf9, Pf10) (Figs. 5, 6). Here, fluvial terraces formed after the retreat of the valley glaciers and hence must be younger than the LGM moraines. This is supported by ^{14}C ages of ca. 8 ka, which Byrd (1995) obtained in the Granite Canyon trench for the fluvial deposits that bury small recessional moraines at the valley mouth. As a consequence, the younger offset river terraces recorded less vertical slip than the moraines around the valley mouth (Fig. 5; Table 1).

Our findings imply that the vertical slip recorded by the Teton fault scarps has accumulated since the end of the Pinedale glaciation and that the oldest geomorphological features yield slip values consistent with a parabolic fault displacement profile (Fig. 7B). At sites where the relative age of the landforms can be determined, the vertical slip correlates with the relative age of the offset geomorphological features, with older geomorphological features showing higher vertical slip than younger landforms. Combined with the available data from moraine systems, lake sediments, and deposits found in the trenches, our results argue against a pre-Pinedale age for the offset geomorphological features, in contrast to the inference by Thackray and Staley (2017). Instead, the lateral variations in fault offsets found by Thackray and Staley (2017) can be mainly explained by their use of the scarp height, which indeed varies considerably along strike of the Teton fault due to the large variations in the far-field slope (Fig. 5; Figs. S1–S4 [footnote 1]). Our analysis, which accounts for the far-field slope when calculating the vertical slip from the vertical separation, shows that our approach yields slip values consistent with a parabolic displacement profile for the oldest landforms.

5.3 Possible Explanations for the Postglacial along-Strike Slip Distribution and Comparison with the Long-Term Displacement Profile

Our results reveal that the postglacial slip distribution along the Teton fault is asymmetric, with the highest vertical slip being found between Jenny Lake

Downloaded from http://pubs.geoscienceworld.org/gsa/geosphere/article-pdf/doi/10.1130/GES02370.1/5364509/ges02370.pdf
by Technische Informationsbibliothek (TIB) user

and the southwestern shore of Jackson Lake (Fig. 7B). We argue that this asymmetry reflects the laterally variable slip rate increase along the Teton fault that was triggered by the melting of the Yellowstone ice cap and Teton Range valley glaciers (Hampel et al., 2007). As shown by the three-dimensional numerical models in Hampel et al. (2007), the northern part of the Teton fault, which was covered by both the Yellowstone ice cap and Teton Range valley glaciers during the Pinedale glaciation (Fig. 1), experienced higher postglacial slip rates than the southern part, which the Yellowstone ice cap did not reach. Alternatively, the asymmetric displacement profile may be related to the transfer of slip to intrabasin faults that occur several kilometers east of the central and southern parts of the Teton fault in its hanging wall (Fig. 3) (Zellman et al., 2019). However, we regard this explanation as unlikely because these intrabasin faults are rather short (to 2–3 km in length) and discontinuous. A preliminary study from the Antelope Flats fault (Fig. 3) showed that the related scarps are not higher than 1–2 m and presumably recorded one post-LGM earthquake (Thackray et al., 2019). Hence, the amount of slip is most likely insufficient to explain the asymmetric displacement profile of the Teton fault. In general, asymmetric fault-displacement profiles may be caused by along-strike variations in rock properties (e.g., Cowie and Scholz, 1992; Schlische et al., 1996; Manighetti et al., 2004) or fault segmentation (e.g., Schwartz and Coppersmith, 1984; Anders and Schlische, 1994; Armstrong et al., 2004). However, the symmetric long-term displacement profile reflected in the topography of the Teton Range (see next paragraph) and the evidence for at least two post-LGM ruptures along the entire Teton fault (Byrd et al., 1994; Larsen et al., 2019; DuRoss et al., 2020, 2021; Zellman et al., 2020) argue against major along-strike variations in rock properties and fault segmentation.

Although the postglacial slip has its maximum north of Jenny Lake, a swath profile along the crest line of the Teton Range (Fig. 7C) suggests a more symmetric displacement profile over a geological time scale, with Jenny Lake and the highest peak (Grand Teton) in the range center. This may indicate that the longer-term slip accumulation is roughly symmetric. As indicated by low-temperature thermochronological data, the Teton fault may have formed at 15–13 Ma and accumulated ~6 km of displacement since then (Brown et al., 2017). Notably, the original Teton fault was probably much longer (as much as 180 km) and potentially linked to the normal fault bounding the Gallatin Range north of the Yellowstone Plateau before its central part was erased by the activity of the Yellowstone hotspot (Brown et al., 2017). Although the timing of the abrupt reduction in fault length remains unconstrained, the shape of the modern Teton Range suggests that there was enough time to develop a symmetric displacement profile as is common for other normal fault–bounded ranges in the northern Basin and Range province (e.g., Densmore et al., 2004).

5.4 Implications for the Postglacial Slip History and Slip Rates

In this section, we discuss the geochronological data that constrain the slip history, the number of earthquakes, and the slip rate of the Teton fault since the retreat of the Pinedale glaciers. At the fault center, the age of the outer moraine around Jenny Lake is constrained by exposure ages for 11 boulders, which yielded an average ^{10}Be age of 15.2 ± 0.7 ka (Licciardi and Pierce, 2018). Assuming that the lateral moraine northwest of Jenny Lake has a similar age, we suggest that the vertical offset of 26.6 ± 2.7 m on profile Pm1 has accumulated in the past ~15 k.y. The nearby profile Pc12 at String Lake yields a similar vertical slip of 25.3 ± 2.5 m and supports this interpretation. In the Jenny Lake area, three other age constraints for the early postglacial history of normal faulting are available. First, the inner Jenny Lake moraine has an average ^{10}Be age of 14.4 ± 0.8 ka (Licciardi and Pierce, 2018). Second, three boulders from the postglacial landslide that transported coarse sedimentary material into Jenny Lake yielded a mean ^{10}Be age of 14.0 ± 0.2 ka (Larsen et al., 2019). Third, a basal 39-cm-thick turbidite layer in Jenny Lake formed at 14.0 ± 0.4 ka (based on radiocarbon dating) and coincides in time with the landslide (Larsen et al., 2019). According to Larsen et al. (2019), the landslide and the corresponding turbidite layer resulted from a major earthquake on the Teton fault at ca. 14 ka. We agree with this interpretation, although we note that the source area of the landslide must be somewhat smaller than inferred by Larsen et al. (2019) because the lateral moraine used for our scarp profile Pm1 is continuous along the entire profile and delimits the northern edge of the (younger) landslide deposits.

Using the postglacial vertical slip of ~27 m and the age of the outer Jenny Lake moraine (ca. 15 ka) results in a time-averaged slip rate of ~1.8 mm/yr for the central Teton fault since 15 ka. Importantly, radiocarbon ages for basin-wide turbidite layers in Jenny Lake suggest that seven major earthquakes occurred between 14 ± 0.4 ka and 7.7 ± 0.1 ka (at an average recurrence interval of 1050 ± 250 yr), whereas only one more earthquake occurred afterwards at ca. 5.3 ka (Larsen et al., 2019). To illustrate that the temporal clustering of earthquakes before 8 ka indicates a pronounced slip-rate decrease through time, we make the following simple calculation. First, we assume that each of the eight documented earthquakes caused the same amount of slip. Hence, the average vertical slip per event is ~3.4 m (i.e., ~27 m of slip divided by eight earthquakes). Second, we separate the postglacial history into two periods of roughly equal length (i.e., 15–8 ka and 8–0 ka). As explained above, six earthquakes occurred in the period 15–8 ka, while only two earthquakes took place between 8 ka and the present. The slip rates for these time intervals are ~2.9 and ~0.85 mm/yr, respectively. Even if these calculations make use of somewhat arbitrarily chosen time intervals, they clearly indicate that the slip rate of the central Teton fault must have markedly decreased during the Holocene.

In the southern part of the Teton fault, paleoseismological investigations at Granite Canyon and Buffalo Bowl revealed altogether three earthquakes that occurred in the last ~10 k.y. (Fig. 3) (Byrd et al., 1994; DuRoss et al., 2020). At the Buffalo Bowl site, Bayesian modeling of radiocarbon and luminescence ages suggests that these events occurred at ca. 9.9 ka, ca. 7.1 ka, and ca. 4.6 ka, again indicating that the slip rate of the fault has significantly decreased during the Holocene (DuRoss et al., 2020). The vertical separation of the displaced alluvial fan, which has been taken as the vertical displacement, is ~6.3 m at

Downloaded from http://pubs.geoscienceworld.org/gsa/geosphere/article-pdf/doi/10.1130/GES02370.1/5364509/ges02370.pdf
by Technische Informationsbibliothek (TIB) user

the Buffalo Bowl trench site (5.9 ± 0.5 m and 6.6 ± 0.3 m on the southern and northern trench walls, respectively; DuRoss et al., 2020). We obtain similar values for Δz from the scarp profiles Pc20 and Pc21 located near Buffalo Bowl (~6.2 m and ~5.1 m). Assuming a fault dip of 60° (Fig. 2A) yields vertical slip values of 7.8 ± 0.8 m and 6.3 ± 0.6 m, respectively, with a weighted mean of 6.8 ± 0.5 m. The vertical slip recorded by fault scarps at the Granite Canyon and Buffalo Bowl trench sites, however, does not reflect the entire postglacial slip of the Teton fault for the following reasons. First, the scarps at both sites postdate the deposition of alluvial sediments, which were dated to be ca. 8 ka at the Granite Canyon trench (Byrd, 1995) and ca. 15 to ca. 10.5 ka at the Buffalo Bowl trench (DuRoss et al., 2020), respectively. Hence, the vertical slip derived from the scarps is related to the Holocene earthquakes observed in the trenches (Byrd, 1995; DuRoss et al., 2020). Second, a comparison with offset river terraces and LGM moraines south of Phelps Lake shows that these fault scarps developed in these landforms recorded 11–12 m (profiles Pf9–Pf10, Pf12) and at least 13–15 m (Pm4–Pm7) of slip, respectively. If the three Holocene earthquakes documented at the two trench sites generated 6–7 m of slip, the remaining slip recorded by the fluvial terraces and moraines must have formed during pre-Holocene earthquakes. From the amount of 11–12 m slip, we infer that the offset river terraces formed after the retreat of LGM valley glaciers but before the formation of the Buffalo Bowl scarp, i.e., most likely between ca. 15 and ca. 10.5 ka. If we assume that the total postglacial slip on the southern Teton fault is ~14 m (based on our profiles Pm4–Pm7), we obtain a time-averaged vertical slip rate of ~0.9 mm/yr over ~15 k.y. (i.e., about half of the rate in the fault center). The difference between the ~7 m of vertical slip at Buffalo Bowl (i.e., ~2.3 m for each of the three earthquakes) derived from our profiles Pc20 and Pc21 and the total slip obtained from profiles Pm4–Pm7 is ~7 m. The latter displacement must have occurred prior to the oldest earthquake recorded in the trench (i.e., before ca. 9.9 ka; DuRoss et al., 2020). If we again consider the time intervals of 15–8 and 8–0 ka as above for the central fault section, ~9.3 m (i.e., two-thirds of the total slip) occurred before 8 ka and ~4.6 m after 8 ka, resulting in slip rates of ~1.3 and ~0.6 mm/yr, respectively. Although these values are based on a limited amount of information, our results suggest that the southern Teton fault has experienced a similar slip-rate decrease as recorded near Jenny Lake. The number of earthquakes in the southern part of the Teton fault remains unknown because events older than 10 ka have not yet been recorded by paleoseismological investigations. If we assume that the fault scarp there also results from eight earthquakes (as at Jenny Lake), the mean vertical slip per event would be 1.8 m, which is similar to the slip inferred from the Granite Canyon and Buffalo Bowl trench sites (Byrd et al., 1994; DuRoss et al., 2020).

A slip rate decrease after the melting of the Yellowstone ice cap is also evident at the northernmost part Teton fault (east of Jackson Lake) when combining the information from our scarp profile Pc1 with the results from the Steamboat Mountain trench site. Here, two earthquakes at ca. 9.7 ka and ca. 5.5 ka produced 4.0 ± 0.5 m of vertical displacement (DuRoss et al., 2021). Our scarp profile Pc1, which is only ~100 m north of the trench site, yields an S_{z_min} to S_{z_max} range of 6.5–9.3 m. Hence, at least 1.5 and as much as 5.3 m of slip accumulated before ca. 10 ka but after the retreat of the Yellowstone ice cap, which entirely covered this area during the LGM. If we assume ~8 m of total postglacial slip and if we consider again the time intervals 15–8 ka and 8–0 ka, the slip rates are 0.86 and 0.25 mm/yr, respectively. If the earthquakes before ca. 10 ka also caused ~2 m of displacement per event (like the events at ca. 9.7 ka and ca. 5.5 ka), then altogether, four postglacial earthquakes have ruptured the northernmost part of the Teton fault.

Combined with the paleoseismological and lake sediment records, our results provide strong evidence that the slip accumulation on the Teton fault has not been uniform through time over the last ~15 k.y. and that a considerable portion of the postglacial slip occurred before ca. 8 ka. Notably, the period of accelerated slip between 15 and 8 ka is observed in all three sections of the fault, which supports the results of Hampel et al. (2007) that about two-thirds of the postglacial slip on the Teton fault occurred between 16 and 8 ka and only one-third between 8 and 0 ka. In accordance with the model predictions, the magnitude of the post-LGM slip rate increase varies along strike of the Teton fault. Considering the time intervals 15–8 ka and 8–0 ka, the slip rate increased by about a factor of ~3 at the northern fault end (Steamboat Mountain) and in the central section (Jenny Lake) and by factor of ~2 in the southern section (Buffalo Bowl). Note that the decrease in the slip rate after the postglacial slip acceleration does not imply that the Teton fault is presently inactive because GPS data clearly show ongoing horizontal extension across the Teton region (Payne et al., 2012).

A still-open question is whether the postglacial slip-rate increase was accomplished by larger displacements per earthquake, an increased number of events, or both. Because the models of Hampel et al. (2007) only captured variations in the fault slip rate, they could not provide information on the number of earthquakes or the slip per event. The rather regular earthquake recurrence interval of 1050 ± 250 yr between 14.0 and 7.7 ka derived from the turbidites in Jenny Lake (Larsen et al., 2019) points to an increased number of earthquakes as the cause for the slip-rate increase, but the slip during these events may have varied too. We envision that the incorporation of the newly available data on the Teton fault earthquake history into future numerical models including earthquake cycles (cf. Bagge et al., 2019) will shed light on this important question.

6. CONCLUSIONS

Our results demonstrate that it is important to account for the far-field slope angle when determining fault slip from scarp profiles, in particular when the offset landforms have relatively steep slopes and/or slope angles differ in hanging wall and footwall. Using the scarp height as a proxy for the vertical slip of normal faults overestimates fault slip, whereas using the vertical separation underestimates the tectonic slip for downhill-facing scarps. As a result, apparent along-strike variations in scarp height or vertical separation

Downloaded from http://pubs.geoscienceworld.org/gsa/geosphere/article-pdf/doi/10.1130/GES02370.1/5364509/ges02370.pdf
by Technische Informationsbibliothek (TIB) user

may not reflect changes in tectonic slip but may rather be related to differences in slope angle. Eliminating the effect of the far-field slope is therefore a necessary precondition for comparing slip estimates from different landforms and for calculating slip rates.

For the Teton fault, our study constrains the along-strike vertical slip distribution of the fault and demonstrates that the tectonic offset recorded by the well-preserved scarps has accrued since the end of the Pinedale glaciation. The obtained vertical displacement profile is asymmetric, with the cumulative post-LGM vertical slip being higher north of the range center than to the south. Combined with the available paleoseismological and lake sediment records, our results provide strong evidence for an accelerated slip accumulation on the Teton fault between ca. 15 and 8 ka, with slip rates being higher in the northern and central fault sections than in the southern section. As shown by earlier numerical models, the laterally variable postglacial slip rate increase and the resulting asymmetric postglacial slip distribution can be explained as a response of the Teton fault to the deglaciation of the Yellowstone-Teton region. To further constrain the postglacial displacement profile and the time interval of accelerated slip, dating of displaced geomorphological features along the Teton fault would be highly desirable.

Based on available constraints on the number of postglacial earthquakes, the average vertical slip per event (~3.4 m) in the central part of the Teton fault indicates that this fault may have ruptured in M_w ~7 earthquakes after the last glacial period (Wells and Coppersmith, 1994). Such a magnitude would be high but not unrealistic, given that the 1959 Hebgen Lake earthquake, which occurred ~130 km northwest of the Teton fault, reached a magnitude of M_w 7.3 (Nishimura and Thatcher, 2003). In the future, we will use the new constraints on the postglacial paleoearthquake history of the Teton fault from Jenny Lake sediment cores (Larsen et al., 2019), the Buffalo Bowl, Leigh Lake, and Steamboat Mountain trench sites (Zellman et al., 2019; DuRoss et al., 2020, 2021), as well as updated ^{10}Be exposure ages on the deglaciation history of the Yellowstone ice cap (Larsen et al., 2016; Licciardi and Pierce, 2018) to investigate the spatio-temporal evolution of slip of the Teton fault in response to the deglaciation of the Teton-Yellowstone region with an updated three-dimensional numerical model that will consider individual paleoseismic events (cf. Bagge et al., 2019).

ACKNOWLEDGMENTS

We thank the editor D. Fastovsky, Associate Editor A. Zuza, T. Stahl, and an anonymous reviewer for their constructive comments, which greatly improved the manuscript. We are grateful to M. Zellman for kindly providing the DEM covering the Teton County Conservation District, and R. Wolff for creating the swath profile in Figure 7C. The publication charge for this article was funded by the Open Access Fund of the Leibniz Universität Hannover.

REFERENCES CITED

Amos, C.B., Burbank, D.W., and Read, S.A.L., 2010, Along-strike growth of the Ostler fault, New Zealand: Consequences for drainage deflection above active thrusts: Tectonics, v. 29, TC4021, https://doi.org/10.1029/2009TC002613.

Anders, M.H., and Schlische, R.W., 1994, Overlapping faults, intrabasin highs, and the growth of normal faults: The Journal of Geology, v. 102, p. 165–179, https://doi.org/10.1086/629661.

Armstrong, P.A., Taylor, A.R., and Ehlers, T.A., 2004, Is the Wasatch fault footwall (Utah, United States) segmented over million-year time scales?: Geology, v. 32, p. 385–388, https://doi.org/10.1130/G20421.1.

Avouac, J.-P., and Peltzer, G., 1993, Active tectonics in southern Xinjiang, China: Analysis of terrace riser and normal fault scarp degradation along the Hotan-Qira Fault System: Journal of Geophysical Research, v. 98, p. 21,773–21,807, https://doi.org/10.1029/93JB02172.

Bagge, M., Hampel, A., and Gold, R.D., 2019, Modeling the Holocene slip history of the Wasatch fault (Utah): Coseismic and postseismic Coulomb stress changes and implications for paleoseismicity and seismic hazard: Geological Society of America Bulletin, v. 131, p. 43–57, https://doi.org/10.1130/B31906.1.

Brown, S.J., Thigpen, J.R., Spotila, J.A., Krugh, W.C., Tranel, L.M., and Orme, D.A., 2017, Onset timing and slip history of the Teton fault, Wyoming: A multidisciplinary reevaluation: Tectonics, v. 36, p. 2669–2692, https://doi.org/10.1002/2016TC004462.

Bucknam, R.C., and Anderson, R.E., 1979, Estimation of fault-scarp ages from a scarp-height–slope-angle relationship: Geology, v. 7, p. 11–14, https://doi.org/10.1130/0091-7613(1979)7<11:EOFAFA>2.0.CO;2.

Byrd, J.O.D., 1995, Neotectonics of the Teton fault, Wyoming [Ph.D. thesis]: Salt Lake City, University of Utah, 214 p.

Byrd, J.O.D., Smith, R.B., and Geissman, J.W., 1994, The Teton fault, Wyoming: Topographic signature, neotectonics, and mechanisms of deformation: Journal of Geophysical Research, v. 99, p. 20,095–20,122, https://doi.org/10.1029/94JB00281.

Caskey, S.J., 1995, Geometric relations of dip slip to a faulted ground surface: New nomograms for estimating components of fault displacement: Journal of Structural Geology, v. 17, p. 1197–1202, https://doi.org/10.1016/0191-8141(95)00023-7.

Cowie, P.A., and Scholz, C.H., 1992, Growth of faults by accumulation of seismic slip: Journal of Geophysical Research, v. 97, p. 11,085–11,095, https://doi.org/10.1029/92JB00586.

Dawers, N.H., Anders, M.H., and Scholz, C.H., 1993, Growth of normal faults: Displacement-length scaling: Geology, v. 21, p. 1107–1110, https://doi.org/10.1130/0091-7613(1993)021<1107:GONFDL>2.3.CO;2.

Densmore, A.L., Dawers, N.H., Gupta, S., Guidon, R., and Goldin, T., 2004, Footwall topographic development during continental extension: Journal of Geophysical Research, v. 109, F03001, https://doi.org/10.1029/2003JF000115.

DuRoss, C.B., Gold, R.D., Briggs, R.W., Delano, J.E., Ostenaa, D.A., Zellman, M.S., Cholewinski, N., Wittke, S.J., and Mahan, S.A., 2020, Holocene earthquake history and slip rate of the southern Teton fault, Wyoming, USA: Geological Society of America Bulletin, v. 132, p. 1566–1586, https://doi.org/10.1130/B35363.1.

DuRoss, C.B., Zellman, M.S., Thackray, G.D., Briggs, R.W., Gold, R.D., and Mahan, S.A., 2021, Holocene paleoseismology of the Steamboat Mountain site: Evidence for full-length rupture of the Teton fault, Wyoming: Bulletin of the Seismological Society of America, v. 111, p. 439–465, https://doi.org/10.1785/0120200212.

Foster, D., Brocklehurst, S.H., and Gawthorpe, R.L., 2010, Glacial-topographic interactions in the Teton Range, Wyoming: Journal of Geophysical Research, v. 115, F01007, https://doi.org/10.1029/2008JF001135.

Gilbert, G.K., 1884, A theory of the earthquakes of the Great Basin, with a practical application [from the Salt Lake Tribune of Sept. 30, 1883]: American Journal of Science, ser. 3, v. 27, p. 49–53, https://doi.org/10.2475/ajs.s3-27.157.49.

Hampel, A., Hetzel, R., and Densmore, A.L., 2007, Postglacial slip rate increase on the Teton normal fault, northern Basin and Range Province, caused by melting of the Yellowstone ice cap and deglaciation of the Teton Range?: Geology, v. 35, p. 1107–1110, https://doi.org/10.1130/G24093A.1.

Hampel, A., Hetzel, R., Maniatis, G., and Karow, T., 2009, Three-dimensional numerical modeling of slip rate variations on normal and thrust fault arrays during ice cap growth and melting: Journal of Geophysical Research, v. 114, B08406, https://doi.org/10.1029/2008JB006113.

Hanks, T.C., and Andrews, D.J., 1989, Effect of far-field slope on morphologic dating of scarp-like landforms: Journal of Geophysical Research, v. 94, p. 565–573, https://doi.org/10.1029/JB094iB01p00565.

Hetzel, R., Tao, M., Stokes, S., Niedermann, S., Ivy-Ochs, S., Gao, B., Strecker, M.R., and Kubik, P.W., 2004a, Late Pleistocene/Holocene slip rate of the Zhangye thrust (Qilian Shan, China) and implications for the active growth of the northeastern Tibetan Plateau: Tectonics, v. 23, TC6006, https://doi.org/10.1029/2004TC001653.

Downloaded from http://pubs.geoscienceworld.org/gsa/geosphere/article-pdf/doi/10.1130/GES02370.1/5364509/ges02370.pdf
by Technische Informationsbibliothek (TIB) user

Hetzel, R., Tao, M., Stokes, S., Niedermann, S., Strecker, M.R., Ivy-Ochs, S., Kubik, P.W., and Gao, B., 2004b, Implications of the fault scaling law for the growth of topography: Mountain ranges in the broken foreland of north-east Tibet: Terra Nova, v. 16, p. 157–162, https://doi.org/10.1111/j.1365-3121.2004.00549.x.

Hoar, R.M., 2019, Refining the onset timing and slip history along the northern part of the Teton fault [M.S. thesis]: Lexington, University of Kentucky, 71 p., https://doi.org/10.13023/etd.2019.021.

Larsen, D.J., Finkenbinder, M.S., Abbott, M.B., and Ofstun, A.R., 2016, Deglaciation and postglacial environmental changes in the Teton Mountain Range recorded at Jenny Lake, Grand Teton National Park, WY: Quaternary Science Reviews, v. 138, p. 62–75, https://doi.org/10.1016/j.quascirev.2016.02.024.

Larsen, D.J., Crump, S.E., Abbott, M.B., Harbert, W., Blumm, A., Wattrus, N.J., and Hebberger, J.J., 2019, Paleoseismic evidence for climatic and magmatic controls on the Teton Fault, WY: Geophysical Research Letters, v. 46, p. 13,036–13,043, https://doi.org/10.1029/2019GL085475.

Licciardi, J.M., and Pierce, K.L., 2008, Cosmogenic exposure-age chronologies of Pinedale and Bull Lake glaciations in greater Yellowstone and the Teton Range, USA: Quaternary Science Reviews, v. 27, p. 814–831, https://doi.org/10.1016/j.quascirev.2007.12.005.

Licciardi, J.M., and Pierce, K.L., 2018, History and dynamics of the Greater Yellowstone Glacial System during the last two glaciations: Quaternary Science Reviews, v. 200, p. 1–33, https://doi.org/10.1016/j.quascirev.2018.08.027.

Love, J.D., 1977, Summary of the Upper Cretaceous and Cenozoic stratigraphy, and of tectonic and glacial events in Jackson Hole, northwestern Wyoming, *in* Heisey, E.L., Lawson, D.E., Norwood, E.R., Wach, P.H., and Hale, L.A., eds., Rocky Mountain Thrust Belt Geology and Resources: Wyoming Geological Association 29th Annual Field Conference Guidebook, p. 585–593.

Love, J.D., Reed, J.C., Jr., and Christiansen, A.C., 1992, Geologic map of Grand Teton National Park: U.S. Geological Survey Miscellaneous Investigations Map I-2031, 1 sheet, scale 1:62,500, https://doi.org/10.3133/i2031.

Love, J.D., Reed, J.C., Jr., and Pierce, K.L., 2003, Creation of the Teton Landscape: Moose, Wyoming, Grand Teton Natural History Association, 132 p.

Machette, M.N., Personius, S.F., Nelson, A.R., Schwartz, D.P., and Lund, W.R., 1991, The Wasatch fault zone, Utah—Segmentation and history of Holocene earthquakes: Journal of Structural Geology, v. 13, p. 137–149, https://doi.org/10.1016/0191-8141(91)90062-N.

Machette, M.N., Pierce, K.L., McCalpin, J.P., Haller, K.M., and Dart, R.L., 2001, Map and data for Quaternary faults and folds in Wyoming: U.S. Geological Survey Open-File Report 2001-461, 154 p., https://doi.org/10.3133/ofr01461.

Mackenzie, D., and Elliott, A., 2017, Untangling tectonic slip from the potentially misleading effects of landform geometry: Geosphere, v. 13, p. 1310–1328, https://doi.org/10.1130/GES01386.1.

Manighetti, I., King, G., and Sammis, C.G., 2004, The role of off-fault damage in the evolution of normal faults: Earth and Planetary Science Letters, v. 217, p. 399–408, https://doi.org/10.1016/S0012-821X(03)00601-0.

Manighetti, I., Campillo, M., Sammis, C., Mai, P.M., and King, G., 2005, Evidence for self-similar, triangular slip distributions on earthquakes: Implications for earthquake and fault mechanics: Journal of Geophysical Research, v. 110, B05302, https://doi.org/10.1029/2004JB003174.

McCalpin, J.P., ed., 2009, Paleoseismology (second edition): New York, Academic Press, International Geophysics Series, v. 95, 613 p.

McCalpin, J.P., and Nishenko, S.P., 1996, Holocene paleoseismicity, temporal clustering, and probabilities of future large (M >7) earthquakes on the Wasatch fault zone, Utah: Journal of Geophysical Research, v. 101, p. 6233–6253, https://doi.org/10.1029/95JB02851.

Morgan, L.A., and McIntosh, W.C., 2005, Timing and development of the Heise volcanic field, Snake River Plain, Idaho, western USA: Geological Society of America Bulletin, v. 117, p. 288–306, https://doi.org/10.1130/B25519.1.

Nishimura, T., and Thatcher, W., 2003, Rheology of the lithosphere inferred from postseismic uplift following the 1959 Hebgen Lake earthquake: Journal of Geophysical Research, v. 108, 2389, https://doi.org/10.1029/2002JB002191.

O'Connell, D.R.H., Wood, C.K., Ostenaa, D.A., Block, L.V., and LaForge, R.C., 2003, Ground motion evaluation for Jackson Lake Dam, Minidoka Project, Wyoming: U.S. Bureau of Reclamation Seismotectonic Report 2003-2, 493 p.

Payne, S.J., McCaffrey, R., King, R.W., and Kattenhorn, S.A., 2012, A new interpretation of deformation rates in the Snake River Plain and adjacent Basin and Range regions based on GPS measurements: Geophysical Journal International, v. 189, p. 101–122, https://doi.org/10.1111/j.1365-246X.2012.05370.x.

Philip, H., Rogozhin, E., Cisternas, A., Bousquet, J.C., Borisov, B., and Karakhanian, A., 1992, The Armenian earthquake of 1988 December 7: Faulting and folding, neotectonics and palaeoseismicity: Geophysical Journal International, v. 110, p. 141–158, https://doi.org/10.1111/j.1365-246X.1992.tb00718.x.

Pierce, K.L., and Morgan, L.A., 2009, Is the track of the Yellowstone hotspot driven by a deep mantle plume? Review of volcanism, faulting, and uplift in light of new data: Journal of Volcanology and Geothermal Research, v. 188, p. 1–25, https://doi.org/10.1016/j.jvolgeores.2009.07.009.

Pierce, K.L., Licciardi, J.M., Good, J.M., and Jaworowski, C., 2018, Pleistocene glaciation of the Jackson Hole area, Wyoming: U.S. Geological Survey Professional Paper 1835, 55 p., https://doi.org/10.3133/pp1835.

Puskas, C.M., Smith, R.B., Meertens, C.M., and Chang, W.L., 2007, Crustal deformation of the Yellowstone–Snake River Plain volcano-tectonic system: Campaign and continuous GPS observations, 1987–2004: Journal of Geophysical Research, v. 112, B03401, https://doi.org/10.1029/2006JB004325.

Roberts, G.P., and Michetti, A.M., 2004, Spatial and temporal variations in growth rates along active normal fault systems: An example from the Lazio-Abruzzo Apennines, central Italy: Journal of Structural Geology, v. 26, p. 339–376, https://doi.org/10.1016/S0191-8141(03)00103-2.

Roberts, S.V., and Burbank, D.W., 1993, Uplift and thermal history of the Teton Range (northwestern Wyoming) defined by apatite fission-track dating: Earth and Planetary Science Letters, v. 118, p. 295–309, https://doi.org/10.1016/0012-821X(93)90174-8.

Schlische, R.W., Young, S.S., Ackermann, R.V., and Gupta, A., 1996, Geometry and scaling relations of a population of very small rift-related normal faults: Geology, v. 24, p. 683–686, https://doi.org/10.1130/0091-7613(1996)024<0683:GASROA>2.3.CO;2.

Schwartz, D.P., and Coppersmith, K.J., 1984, Fault behavior and characteristic earthquakes: Examples from the Wasatch and San Andreas fault zones: Journal of Geophysical Research, v. 89, p. 5681–5698, https://doi.org/10.1029/JB089iB07p05681.

Smith, R.B., Byrd, J.O.D., and Susong, D.D., 1993, The Teton fault, Wyoming: Seismotectonics, Quaternary history, and earthquake hazards, *in* Snoke, A.W., Steidtmann, J.R., and Roberts, S.M., eds., Geology of Wyoming: Geological Survey of Wyoming Memoir 5, p. 628–667.

Thackray, G.D., and Staley, A.E., 2017, Systematic variation of Late Pleistocene fault scarp height in the Teton Range, Wyoming, USA: Variable fault slip rates or variable landform ages?: Geosphere, v. 13, p. 287–300, https://doi.org/10.1130/GES01320.1.

Thackray, G.D., DuRoss, C.B., Zellman, M., Wittke, S.J., Gold, R.D., Delano, J.E., Jobe, J.A.T., Hille, M., Grasso, K., and Mahan, S.A., 2019, Is the Antelope Flats fault an antithetic rupture of the Teton fault? [abstract]: Seismological Research Letters, v. 90, p. 901–902.

Thompson, S.C., Weldon, R.J., Rubin, C.M., Abdrakhmatov, K., Molnar, P., and Berger, G.W., 2002, Late Quaternary slip rates across the central Tien Shan, Kyrgyzstan, central Asia: Journal of Geophysical Research, v. 107, 2203, https://doi.org/10.1029/2001JB000596.

Wells, D.L., and Coppersmith, K.J., 1994, New empirical relationships among magnitude, rupture length, rupture width, rupture area, and surface displacement: Bulletin of the Seismological Society of America, v. 84, p. 974–1002.

Wessel, P., Smith, W.H.F., Scharroo, R., Luis, J., and Wobbe, F., 2013, Generic Mapping Tools: Improved version released: Eos (Transactions, American Geophysical Union), v. 94, p. 409–410, https://doi.org/10.1002/2013EO450001.

White, B.J.P., Smith, R.B., Husen, S., Farrell, J.M., and Wong, I., 2009, Seismicity and earthquake hazard analysis of the Teton–Yellowstone region, Wyoming: Journal of Volcanology and Geothermal Research, v. 188, p. 277–296, https://doi.org/10.1016/j.jvolgeores.2009.08.015.

Zellman, M.S., DuRoss, C.B., and Thackray, G.D., 2019, The Teton fault: Wyoming Geological Survey Open-File Report 2019-1, scale 1:75,000.

Zellman, M.S., DuRoss, C.B., Thackray, G.R., Personius, S.F., Reitman, N.G., Mahan, S.A., and Brossy, C.C., 2020, Holocene rupture history of the central Teton fault at Leigh Lake, Grand Teton National Park, Wyoming: Bulletin of the Seismological Society of America, v. 110, p. 67–82, https://doi.org/10.1785/0120190129.

Downloaded from http://pubs.geoscienceworld.org/gsa/geosphere/article-pdf/doi/10.1130/GES02370.1/5364509/ges02370.pdf
by Technische Informationsbibliothek (TIB) user